The Thesis Committee for Michael David Aman
Certifies that this is the approved version of the following thesis:

Micromechanical Testing for the Evaluation of Chemo-Mechanical Alteration of CO_2 Storage Rocks

APPROVED BY
SUPERVISING COMMITTEE:

Supervisor: _____
D. Nicolas Espinoza

_____
Matthew T. Balhoff

Micromechanical Testing for the Evaluation of Chemo-Mechanical Alteration of CO_2 Storage Rocks

by

Michael David Aman, B.S.

Thesis

Presented to the Faculty of the Graduate School of

The University of Texas at Austin

in Partial Fulfillment

of the Requirements

for the Degree of

Master of Science in Engineering

The University of Texas at Austin

May 2017

Dedication

To my family

Acknowledgements

I would like to acknowledge my thesis advisor, Dr. D. Nicolas Espinoza, for his continued support, guidance and words of encouragement in accomplishing this work and my graduate degree.

I would like to thank Dr. Matthew T. Balhoff for providing his time and insight as the second reader of this thesis report.

I would like to acknowledge Jonathan Major and Dr. Peter Eicchubl for providing the rock samples from the Crystal Geyser site and relevant mineral composition data, without which the research would not have been possible. I would like to thank Darryl Nygaard for extensive support with fabrication and equipment design. I would like to acknowledge Luis Hernandez-Uribe for assistance with autoclave experiments. I would like to thank Jessica Kruichak and Melissa Mills from Sandia National Laboratories for help with collecting ion chromatography and BET data.

This work was supported as part of the Center for Frontiers of Subsurface Energy Security, an Energy Frontier Research Center funded by the U.S. Department of Energy, Office of Science, Basic Energy Sciences under Award DE-SC0001114. I would like to thank Dr. Anastasia Ilgen and Dr. Susan Altman for the opportunity to collaborate and conduct research at Sandia National Laboratories. Sandia National Laboratories is a multi-mission laboratory managed and operated by Sandia Corporation, a wholly owned subsidiary of Lockheed Martin Corporation, for the U.S. Department of Energy's National Nuclear Security Administration under contract DE-AC04-94AL85000.

Abstract

Micromechanical Testing for the Evaluation of Chemo-Mechanical Alteration of CO_2 Storage Rocks

Michael David Aman, M.S.E.

The University of Texas at Austin, 2017

Supervisor: D. Nicolas Espinoza

This thesis investigates the relationship between the chemically and mechanically coupled alteration of CO_2-storage rocks during CO_2 geological storage and the ensuing changes in rock properties. I analyzed how the scratch toughness and hardness varied with alteration by CO_2-fluid mixtures by employing indentation and scratch test methodologies. Rock samples were selected from the Crystal Geyser site near Green River Utah, where a natural seepage of CO_2 altered outcrops of the Entrada sandstone and Summerville siltstone formations near faults over tens of thousands of years. Results from tests on Entrada sandstone and Summerville siltstone from the Crystal Geyser site show that mechanical parameters measured with indentation (indentation hardness, Young's modulus and contact creep compliance rate) and scratching (scratch hardness and scratch toughness) consistently indicated weakening of the rock after CO_2-induced alteration. Decreases of measured parameters vary from 14% to 87%. In order to investigate the time scales of variation of mechanical and petrophysical properties differing to those before exposure, I

conducted autoclave reaction experiments with Entrada sandstone and Summerville siltstone exposed to either de-ionized water or synthetic brine under reservoir pressure (9-10 MPa) and temperature (80°C) conditions for up to two weeks. I designed and constructed a scratch testing apparatus to conduct scratches on the laboratory altered rock samples. Scratch toughness and hardness show decreases of up to 60% in the case of Entrada sandstone and 92% in the case of Summerville siltstone after CO_2-induced alteration in the laboratory. To understand chemical reactions during the laboratory alteration experiments, I conducted parallel experiments using powdered samples of Entrada sandstone and Summerville siltstone. I quantified aqueous ion concentrations for fluid samples collected from these autoclave experiments using analytical geochemistry. Dissolution of calcite and silicate cements are the primary reactions identified for both samples during the laboratory experiments. Recognizing the susceptibility of rock facies to CO_2-related alteration at target CO_2 geological storage formations is critical to ensuring the long-term mechanical stability and security of CO_2 trapping.

Table of Contents

List of Tables

List of Figures

List of Illustrations

1. Introduction

1.1 BACKGROUND

Geological storage of carbon dioxide (CO_2) is a rapidly developing technology, which can potentially limit the increase in atmospheric CO_2 concentration. Understanding the coupled chemical and mechanical interactions between the injected CO_2 and reservoir rock is critical to the long-term prediction of storage efficiency and the structural integrity of geological CO_2 storage formations. Field and laboratory studies have documented of dissolution of injected CO_2 into reservoir brine, resulting in brine acidification and shifts in chemical equilibrium (Kaszuba et al., 2005; Carroll et al., 2011; Lu et al., 2012). The resulting reactive CO_2-brine mixture may induce dissolution and secondary reprecipitation of load carrying mineral phases. Reactivity may differ between sites depending on the rock and brine composition, though carbonate minerals are characterized by faster dissolution kinetics compared to silicates (Stumm and Morgan, 1996; Pokrovsky et al., 2005; Le Guen et al., 2007). Long-term exposure to CO_2-brine mixtures has been shown to alter the transport and mechanical properties of reservoir rocks, particularly for rocks with considerable carbonate content (Rohmer et al., 2016; Sun et al., 2016). Changes in mechanical properties can affect the reservoir's response to *in situ* stresses with undesirable implications for caprock and well casing integrity.

Laboratory scale experiments have confirmed model-based evidence for the mechanical weakening of reservoir rock with exposure to CO_2-acidified brine and subsequent mineral dissolution. Specifically, CO_2 alteration of rock cores has resulted in increases in permeability and porosity (Canal et al., 2013), dissolution of siliceous and

carbonate minerals (Carroll et al., 2013), reduction of fracture toughness (Major et al., 2014), and decrease of the size of yield stress locus (Rinehart et al., 2016). Additionally, evidence for local degradation of mechanical properties has implications for reservoir scale processes. Coupled chemo-mechanical models have shown that mineral dissolution in the context of CO_2 sequestration may result in a decrease in horizontal effective stress, potentially resulting in either compaction-driven shear failure or stress intensification in the caprock (Kim & Santamarina, 2014). However, difficulty remains in the practicality of carrying out laboratory alteration experiments with rocks and CO_2-fluid mixtures and the ability to predict reservoir behavior based on laboratory results.

While the majority of previous experimental work has been conducted on the core (centimeter) scale specimen utilizing core holders and autoclave reactors, CO_2-brine alteration experiments are limited by their practical duration. For a one-month autoclave batch experiment, the reaction front in a core of rock would be expected to penetrate the surface at a distance on the scale of millimeters. The potential effect of the reacted "skin" on the bulk strength of the core would be limited, rendering traditional rock mechanics tests, such as unconfined compressive strength testing, triaxial testing and elastic wave velocity measurement, ineffective. Micromechanics tests such as the indentation test and the scratch test offer a practical alternative by preferentially probing the reacted and unaltered regions.

In order to evaluate the mechanisms of alteration for a given laboratory experiment, microscopy, analytical and model-based geochemical techniques can be employed. Laboratory derived dissolution rate equations, rate constants, and activation energies from batch experiments with minerals and rocks can be used to describe the dissolution for a

given mineral in a distinct rock type, but the laboratory-derived mineral dissolution rates can be orders of magnitude faster than those observed in the field (Carroll et al, 2013). Experiments using mineral powders are useful as a first step towards investigation of mineral reaction mechanisms and kinetics, while giving the advantage of shorter run times (Lüttge & Metz, 1993).

The defined research topic was proposed to analyze the relationship between scratch toughness, hardness, Young's modulus, and creep for reservoir rocks and duration of alteration by CO_2-charged fluids in field and laboratory contexts. I selected Entrada sandstone and Summerville siltstone core samples taken from the Crystal Geyser site near Green River, Utah, to provide mechanical testing results analogous to what might be expected from a CO_2 injection field site. These formations were altered locally by CO_2 charged brines over approximately 100,000 years (Burnside, 2010). I reproduced reactions similar to those that occurred at the field site in laboratory autoclave experiments with the Entrada sandstone and Summerville siltstone rocks in core and powder form. Experiment conditions model the field site through use of synthetic brine based on the groundwater chemistry at Crystal Geyser and pressure and temperature conditions typical of CO_2 storage reservoirs (9.3 MPa and 80°C). I used altered and unaltered rock cores for indentation and scratch testing. The mechanical parameters obtained are compared against unaltered field samples and field samples taken from regions where the Crystal Geyser CO_2 seepage is present. I altered powdered rock samples of the Entrada sandstone and Summerville siltstone to reveal information of the mechanisms of alteration in the experiments through the employment of inductively coupled plasma mass-spectrometry and ion

chromatography in combination with microscopy. The primary reactions identified are the dissolution of calcite and silicate based cements.

1.2 THESIS ORGANIZATION

This thesis is organized in 6 chapters. Chapter 1 introduces the reader to the topics of geomechanics and geochemistry in the context of CO_2 geological storage. This chapter gives information on the current state of laboratory experiments investigating the alteration of storage rocks by CO_2-fluid mixtures and the geochemical and geomechanical changes induced by that alteration. The application of micromechanical testing to rocks altered over laboratory time scales is introduced.

Chapter 2 gives details on the geology of the Entrada sandstone and Summerville siltstone rock samples collected for and examined in this thesis. Details on the methodology of the scratch and indentation tests utilized in this thesis are provided. This chapter informs the method of calculation of the Young's modulus, contact creep compliance rate, and indentation hardness from an indentation test. Additionally, information on the calculation of the scratch toughness and scratch hardness from a scratch test is given.

Chapter 3 details the construction process of an apparatus for the completion of scratch tests. Information on specific components and the design process is given. Additionally, this chapter details the successful validation of the completed device through the calculation of fracture toughness on several reference materials. Criteria for the accurate interpretation of scratch toughness from scratch test results are described.

Chapter 4 describes the results from indentation tests completed on Entrada sandstone and Summerville siltstone samples taken from the Crystal Geyser site near Green

River, Utah, where rock near faults and veins has been bleached by CO_2 seepages. Results include the variation of Young's modulus, indentation hardness and contact creep compliance rate. Young's modulus decreased by 23% and 51% for the bleached Entrada sandstone and Summerville siltstone relative to unaltered cores, respectively. Hardness decreased by 38% and 25% for the bleached Entrada sandstone and Summerville siltstone, respectively. Contact creep compliance rate increased by 72% and 160% for the bleached Entrada sandstone and Summerville siltstone, respectively. This work has been published in Sun et al., 2016.

Chapter 5 details the alteration of Entrada sandstone and Summerville siltstone in core and powdered form in autoclave reactions with supercritical CO_2-fluid mixtures. The results of scratch tests conducted on the altered core samples are reported and the determined scratch toughness and hardness values are compared with the unaltered and bleached field samples. Scratch toughness and hardness show decreases of up to 60% in the case of Entrada sandstone and 89% in the case of Summerville siltstone after CO_2-induced alteration in the laboratory. Powdered sample experiments are used to facilitate the sampling of aqueous solutions for analytical geochemistry and the results of inductively coupled plasma mass spectrometry and ion chromatography on aqueous solutions collected at intervals during the powdered sample autoclave experiments are reported. Results demonstrate that the dissolution of silicate and calcite based cement is the primary reaction occurring in the autoclave experiments. This study has been submitted to a peer-reviewed journal under the title "Characterization of Chemo-Mechanical Alteration in CO_2 Storage Rocks via Scratch Testing."

Finally, Chapter 6 concludes the thesis summarizing the above results. Limitations of the application of the results observed in this thesis to reservoir scale phenomena are described. This chapter gives recommendations on the potential improvement of the methodology employed in this thesis by increasing the fidelity of the scratch apparatus or modifying the autoclave alteration experiments to better represent reservoir process with more realistic fluid to rock ratios.

2. Experimental Background

2.1 GEOLOGY

At the Crystal Geyser site near Green River, Utah, a CO_2 seepage has existed along the Little Wash and Salt Wash grabens for tens of thousands of years (Burnside, 2010). Nearby the faults, fractures and veins at this field site, the Entrada sandstone and the Summerville siltstone, both Middle Jurassic sandstones (Doelling, 2001), have been bleached by CO_2 charged fluids.

The Entrada sandstone is an Aeolian dune deposit characterized by red-brown, silty, and fine grains. The Summerville Formation is composed of red-brown siltstone, sandstone and gypsum (Doelling, 2001). Both sandstones used in this study are primarily quartz based, with carbonate based cement, including calcite and dolomite, as shown in Table 1. The Entrada sandstone resembles a typical sandstone reservoir rock while the Summerville siltstone exhibits features of a moderate seal rock.

Table 2.1: Mineral composition of unbleached Entrada sandstone and Summerville siltstone samples analyzed by X-ray diffraction (Major et al., 2014).

Mineral	Unaltered Entrada sandstone (wt %)	Unaltered Summerville siltstone (wt %)
Quartz	46%	53%
Calcite	9%	29%
Illite-Smectite	21%	8%
Dolomite	9%	0%
Kaolinite	6%	0%
Orthoclase	4%	2%
Aragonite	0%	6%
Albite	2%	2%
Ankerite	2%	0%
Hematite	Trace[a]	0%

[a]Hematite grain coatings observed in SEM images of thin sections

2.2 MICROMECHANICAL TESTING

Micro-indentation and scratching tests target a probed volume smaller than ~1 mm^3. They are employed frequently in materials testing and recently in the mechanical evaluation of petroleum rocks (Richard et al., 1998; Schei et al., 2000).

2.2.1 Scratch Testing

The scratch test measures the resistance of a flat, polished sample to surface damage induced from a scratch imposed with a stylus of known geometry moved at constant speed and normal force (ASTM G171) along the sample's surface. A measure of the scratch hardness and fracture toughness can be calculated from the normal load, tangential load, and residual shape of the scratch (ASTM G171, Akono & Ulm, 2011).

For scratch tests conducted on rocks, experiments target a contact area several times larger than the grain size such that the measured mechanical properties reflect the bulk properties of the cemented rock matrix rather than the properties of a single grain.

The scratch test allows the calculation of scratch hardness $H_{scratch}$ and scratch toughness K_c (this latter if testing conditions are appropriate). Transverse force F_T induced by the scratch stylus on the sample surface and lateral displacement are recorded during the scratch test under a constant normal force F_v. The scratch width w is usually determined through a geometrical transformation of the scratch depth. Alternatively, the scratch width can be determined or validated with post-experiment surface inspection and image analysis. The scratch hardness is calculated according to ASTM G171 as

$$H_{scratch} = \frac{kF_v}{w^2}, \tag{2.1}$$

where k is a geometric constant. Figure 2.1 shows a representative plot of the data acquisition during a scratch test and the subsequently determined scratch toughness and hardness plotted along the scratch path.

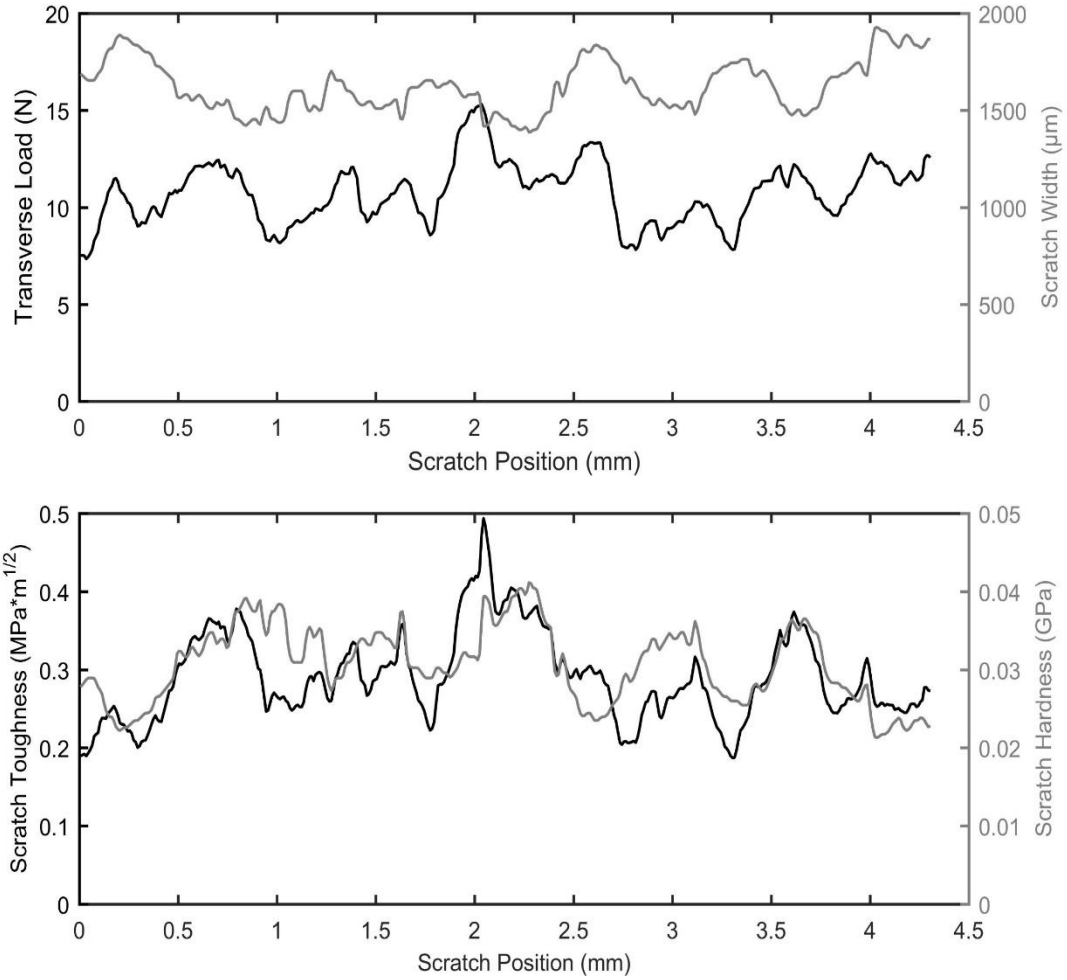

Figure 2.1: Raw data (top) and calculated parameters (bottom) for a 30 N normal load scratch conducted on Summerville siltstone altered for one week in a synthetic brine-supercritical CO_2 mixture.

Scratch toughness K_c [MPa·m$^{1/2}$] is calculated as follows (Akono et al., 2011; Akono & Ulm 2012),

$$K_c = \frac{F_T}{\sqrt{2pA}}, \tag{2.2}$$

where F_T is the transverse force, p is the horizontal projected scratch perimeter and A is the horizontal projected load bearing contact area. Parameters p and A are a function of the scratch width and stylus shape. For a stylus of known geometry, such as a spherical-conical tipped stylus, the indenter shape function $2pA$ can be approximated through individual calculation of p and A, which vary with depth of scratch. Equation 2.2 is valid for depths of scratch sufficient for the $F_T/\sqrt{2pA}$ relationship to approach a constant value, which occurs at a depth proportional to the material's internal length scale (Akono et al., 2012).

2.2.2 Indentation Testing

Indentation tests involve applying a normal load on the flat surface of a sample with an indenter tip of known geometry. The penetration of the indenter tip causes both elastic and plastic deformation of the sample. When reaching a preset maximum load value, the normal load is reduced until partial or complete relaxation occurs. The resulting load/displacement curve provides data related to the mechanical nature of the material (Cripps, 2011).

A representative plot of the data output from a single indentation test on an unaltered Entrada sandstone sample is shown in Figure 2.2. The simplest direct output from the example curve in Fig. 1 is the maximum indentation depth h_{max} at the preset maximum applied load P_{max}. The stiffness S is calculated from a fit of the upper one third of the unloading curve. These three parameters enable an estimation of the contact depth h_c,

$$h_c = h_{max} - \frac{3P_{max}}{4S}. \quad (2.3)$$

For a perfect Vickers indenter, an estimate of the projected contact area A_c is provided by the indenter shape function,

$$A_c = 24.5h_c^2. \quad (2.4)$$

An experimentally determined estimation of the indenter shape function would be recommended to ensure the properties measured during the indentation test are indeed characteristic of the material. However, Equation 2.4 provides a rough estimate for an ideal Vicker's indenter sufficient for comparison of properties measured with the same apparatus.

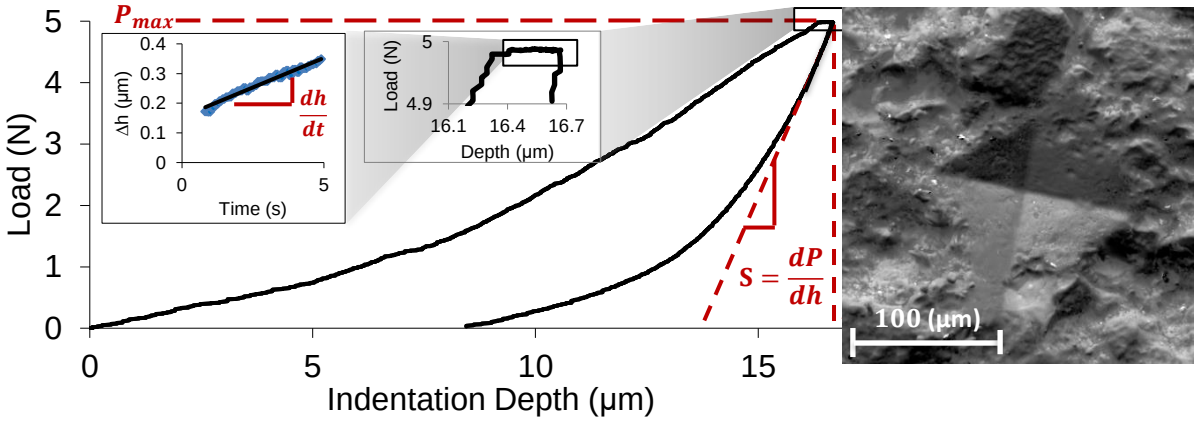

Figure 2.2: (Left) representative loading and unloading curve for an indentation test on unaltered Entrada sandstone.

ASTM E2546 provides the equations for computing indentation hardness H_I [GPa], the reduced modulus E_r [GPa], and Young's modulus E [GPa],

$$H_I = \frac{P_{max}}{A_c}, \tag{2.5}$$

$$E_r = \frac{\sqrt{\pi}}{2}\frac{S}{\sqrt{A_c}}, \tag{2.6}$$

$$E = (1-\upsilon^2)\left(\frac{1}{E_r} - \frac{1-\upsilon_i^2}{E_i}\right)^{-1}, \tag{2.7}$$

where E_i and υ_i are the Young's modulus and Poisson's ratio of the indenter tip (NIST Ceramics gives a standard diamond E_i = 1140 GPa and υ_i = 0.07) and υ is the Poisson ratio of the tested sample. We assumed υ = 0.2 for the tested clastic rock samples.

The contact creep compliance rate $\dot{L}$ [(GPa·s)$^{-1}$], a measure of the time-dependent response of the material to a step load, is given by

$$\dot{L} = \frac{2a_U \frac{dh}{dt}}{P_{max}}, \tag{2.8}$$

where a_U is the contact radius at the beginning of the unloading phase and dh/dt is the change in indentation depth with respect to time. The derivation of this equation, detailed by Vandamme et al. (2012), takes into account plasticity under the indentation tip encountered during the loading phase. The measure is independent of loading profile and indenter geometry. Figure 2.2 shows an inset with a zoom of the creep region from where dh/dt is obtained using a linear fit.

3. Scratch Testing Apparatus

3.1 CONSTRUCTION

A state-of-the-art scratch testing device was designed for the purposes of the study. The scratch tester consists of a 9064-XY translation stage (Newport Corp.) with a mounted sample vise, a micrometer connected by pulley to a NEMA 17 stepper motor for controlled horizontal translation, and an instrumented motor-controlled stylus with a diamond tipped conical-spherical probe (Gilmore Diamond Tools, Inc.), as shown in Fig. 1. Horizontal position and force measurement was achieved through the implementation of a LDI-119 linear variable differential transformer (Omega Engineering) and a LC302 load cell (Omega Engineering) mounted in-line with the actuating micrometer and stage. The vertical load was applied with a fixed weight applied to the stylus. The stylus, when loaded, was constrained to move under vertical translation only. Electronic motor and force transduction components were interfaced with LabView software through an Arduino Uno board for control and an Agilent 34972A data acquisition system.

A schematic of the scratch testing device design is shown in Figure 3.1. A simplified two dimensional view shows the relative positions of components. Arrows show the degrees of freedom of movement in mobile components. Design sketches for individually fabricated components are available in Appendix C.

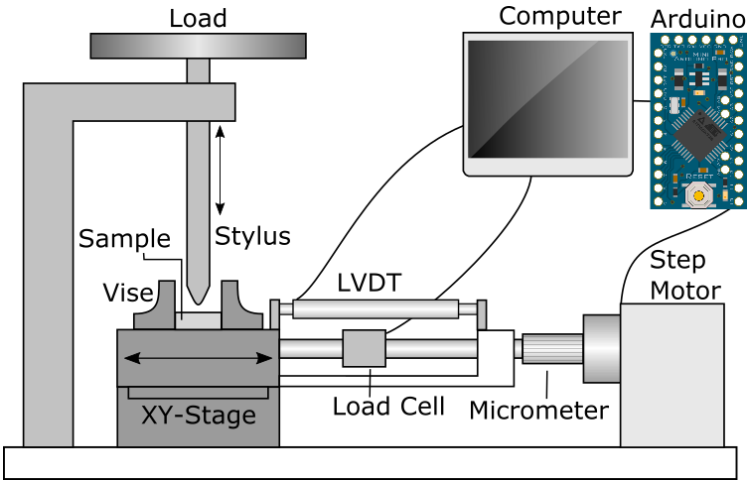

Figure 3.1: Schematic drawing of the scratch device components

The scratch testing device is capable of applying constant normal loads of up to 25 lb to the sample through its vertical stylus. The LDI-119 linear variable differential transformer in use has a measurement range of 25 mm full scale, with a linearity error of 0.15% of full scale output and a resolution of 0.025% of full scale. The load cell in use has a 100 N range with an accuracy (linearity, hysteresis and repeatability combined) of 0.5% of full scale output. A photograph of the scratch testing apparatus is shown in Figure 3.2.

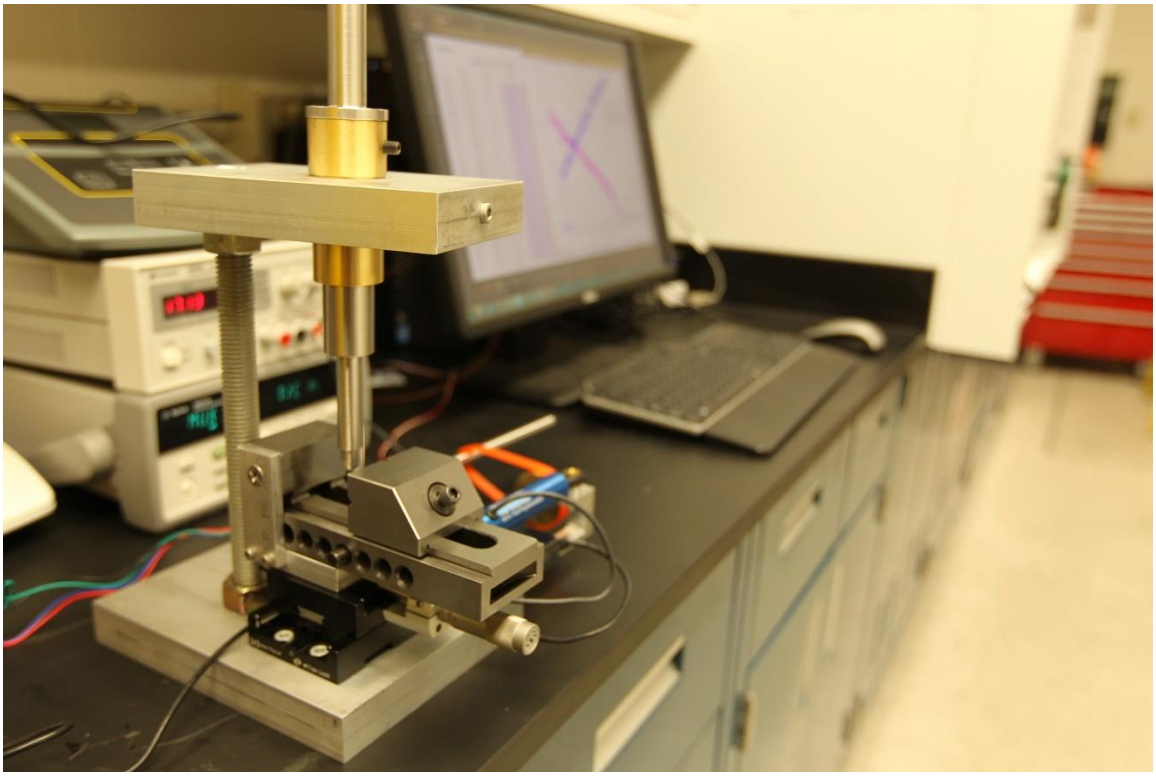

Figure 3.2: Photograph of the scratch device

3.2 Device Validation

In order to confirm the accuracy of the scratch toughness measurements, I conducted scratch tests on pyrex and soda lime glass, whose fracture toughness is readily available in the literature. Pyrex has a fracture toughness of 0.63 $MPa \cdot m^{1/2}$ and soda lime glass has a fracture toughness of 0.70 $MPa \cdot m^{1/2}$ (Harding et al., 1994). The scratch test results showed a scratch toughness of 0.65±0.12 $MPa \cdot m^{1/2}$ and 0.72±0.13 $MPa \cdot m^{1/2}$ for pyrex and sodalime glass, respectively. Scratch toughness for one of each scratch for pyrex and soda lime glass are plotted in Figure 3.3. Given the relative error of averaged scratch toughness measurements across a scratch performed on a heterogeneous rock sample, the

minor discrepancy in the glass scratch toughness measurements was determined to be acceptable.

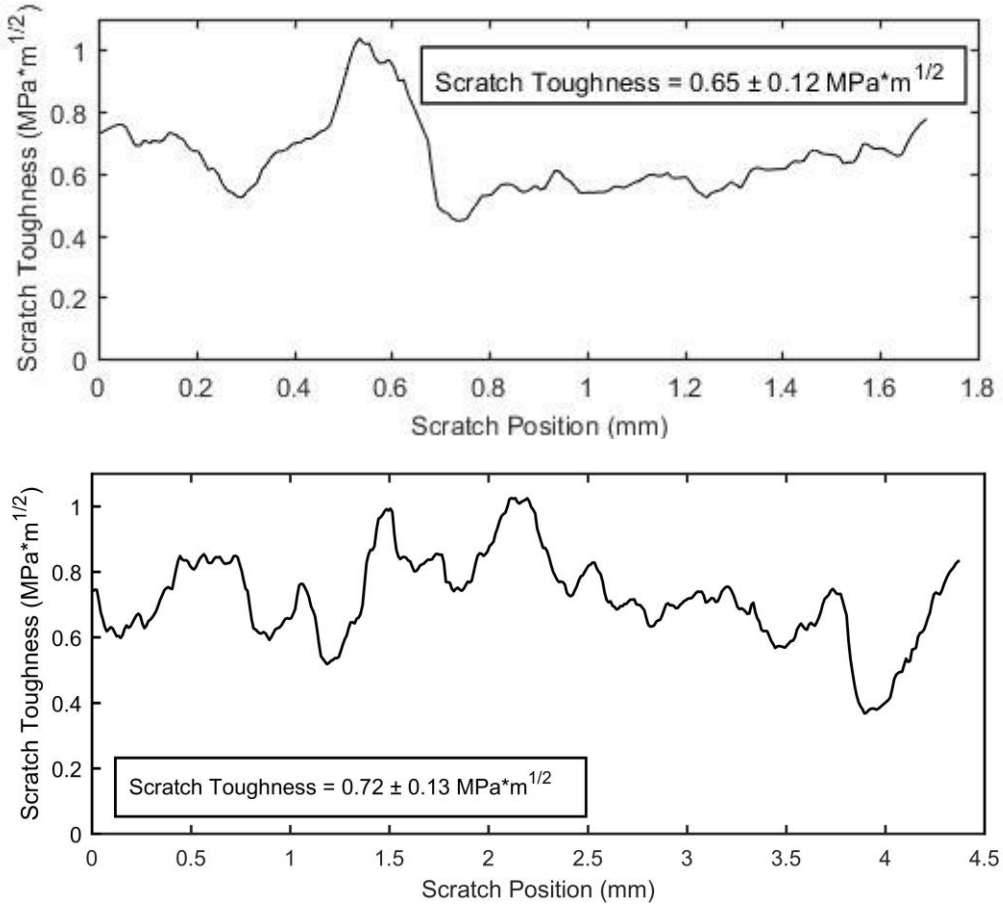

Figure 3.3: Scratch toughness results for scratches conducted on pyrex (top) and soda lime glass (bottom).

Micromechanical experiments must consider the internal length scales of the tested geological samples. The objective is to test a representative volume that can inform about the effect of CO_2-acidified brine on the rock matrix including the impact of cementation at contacts if any. For indentation, let us consider the ratio between the projection of the

probed area A_c and the average cross sectional area of a grain ~$(d_{50})^2$ as an indicator of relative length scales. In the indentation tests for the Entrada sandstone and the Summerville siltstone, the ratio $A_c/(d_{50})^2$ varies from 1 to 10 and from 18 to 100, respectively for a maximum indentation depth of 35 μm. For this scenario, it likely that grain scale heterogeneity would impact the indentation results by increasing variability of measurements.

Similarly, scratch tests must consider the internal length scales of rock samples. At low penetration depths, materials may behave with more of a ductile response not representative of their true fracture toughness at higher penetration depths. Akono et al. (2012) indicates that a plot of F_t versus $\sqrt{2pA}$, whose slope is equivalent to apparent scratch toughness, approaches a horizontal asymptote representing the fracture toughness after exceeding a certain ratio of d/R, where d is scratch depth and R is the indenter tip radius. Without the implementation of load and displacement controlled penetration, I estimated the approximate value of the dimensionless internal length scale d/R for the Entrada sandstone and Summerville siltstone by conducting scratches at progressively higher constant vertical loads. Scratch tests completed above the dimensionless internal length scale should estimate the true scratch toughness of the material. The dimensionless internal length scale was estimated at 0.5 for both the Entrada sandstone and Summerville siltstone, with a corresponding indenter tip radius of 200 μm.

In experiments where sufficient friction exists at the stylus-sample interface, no slippage should occur and the beam should remain perpendicular to the sample surface. Practically, the materials tested responded at times to the probe with stick-slip behavior due to the removal of material by brittle chipping. One potential drawback of this design

is that slippage along the stylus contact may cause deviation from a perfectly lateral scratch path or non-vertical application of force to the surface. The scratch model used necessarily assumes that the stylus is vertical with respect to the surface, so non-perpendicular application of stylus load increases error in measurement of mechanical properties. The rigidity of the system may be optimized by reducing the length of the stylus beam or changing the material of the beam.

4. Micromechanical Testing of Crystal Geyser Field Samples

4.1 METHODOLOGY

Entrada sandstone and Summerville siltstone from Crystal Geyser, Utah were tested. The grain sizes vary from 50-100 μm for Entrada sandstone and 5-20 μm for Summerville siltstone. The outcrops in some parts have been altered (bleached) by natural leakage of CO_2-charged brine. The alteration was characterized by dissolution and reprecipitation of carbonates, clays and iron cements (further details available in Wigley et al., 2012 and Major et al., 2014). I tested both CO_2-altered and unaltered samples provided by J. Major and P. Eichhubl. Therefore, four samples are considered: unaltered Entrada sandstone, CO_2-altered Entrada sandstone, unaltered Summerville siltstone and CO_2-altered Summerville siltstone.

The samples were cut into 1 in cubes using a diamond saw for the indentation test. For the scratch test, the samples were drilled perpendicular to their bedding planes, producing cylindrical cores of 1 cm diameter. In both cases, one surface parallel to the bedding plane was polished with Allied Tech diamond lapping film on a lapping wheel to a desired surface roughness suitable to obtain reliable experimental results (according to Miller et al., 2008, the root-mean-squared roughness of the sample should be less than five times of the average penetration depth).

4.1.1 Indentation

A Nanovea PB1000 device was used to perform the indentation tests. A standard Vicker's indenter was driven into the polished sample surface at a loading rate of 10 N/min. After the pre-set maximum load of 5 N was reached, the applied load was held and paused

for 5 seconds. The non-contact optical sensor keeps recording any time-dependent creep response of the sample at this stage. After 5 seconds, the indenter tip was lifted with an unloading rate of 10 N/min. Indentation depth on the sample surface was recorded throughout the entire loading/unloading process. The recorded signal is plotted against the corresponding applied load for analysis.

4.2 RESULTS

Five indentation tests were performed on each of the four rock samples. Figure 4.1 shows the results for the 20 indentation tests performed. The maximum indentation depth ranges from ~15 to 30 μm in Entrada Sandstone and from ~15 to 35 μm in Summerville siltstone. Hence, the contact area varies from about 5500 μm^2 to 30,000 μm^2, which in the case of Entrada sandstone is equivalent to approximately 1 to 10 times the cross sectional area of a sand grain. CO_2-altered samples tend to show higher maximum indentation depths and less steep elastic rebound than the unaltered samples. Differences in indentation hardness are discernible in Figure 4.1 through corresponding differences in mean indentation depths between samples.

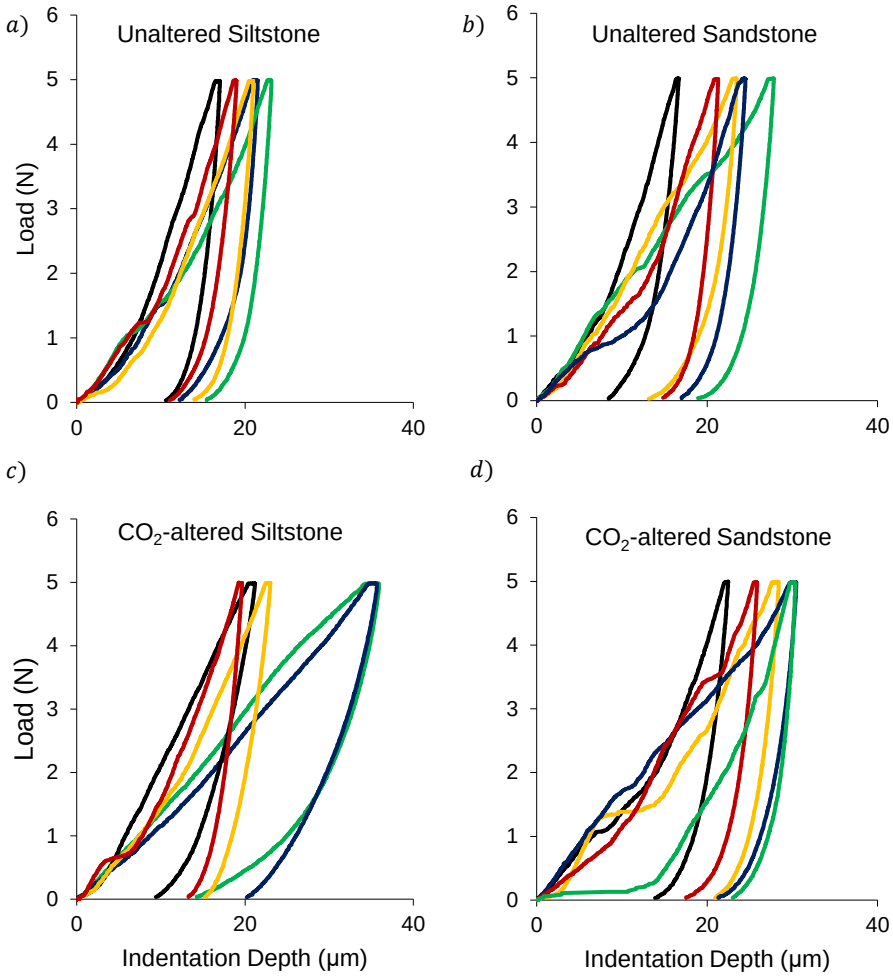

Figure 4.1: Indentation loading/unloading curves for (a) unaltered Summerville siltstone, (b) unaltered Entrada sandstone, (c) CO_2-altered Summerville siltstone, and (d) CO_2-altered Entrada sandstone.

Figure 4.2 shows the average and 95% confidence intervals (as error bars) of indentation hardness, Young's Modulus, and creep compliance rate computed with Equations 2.5-2.8.

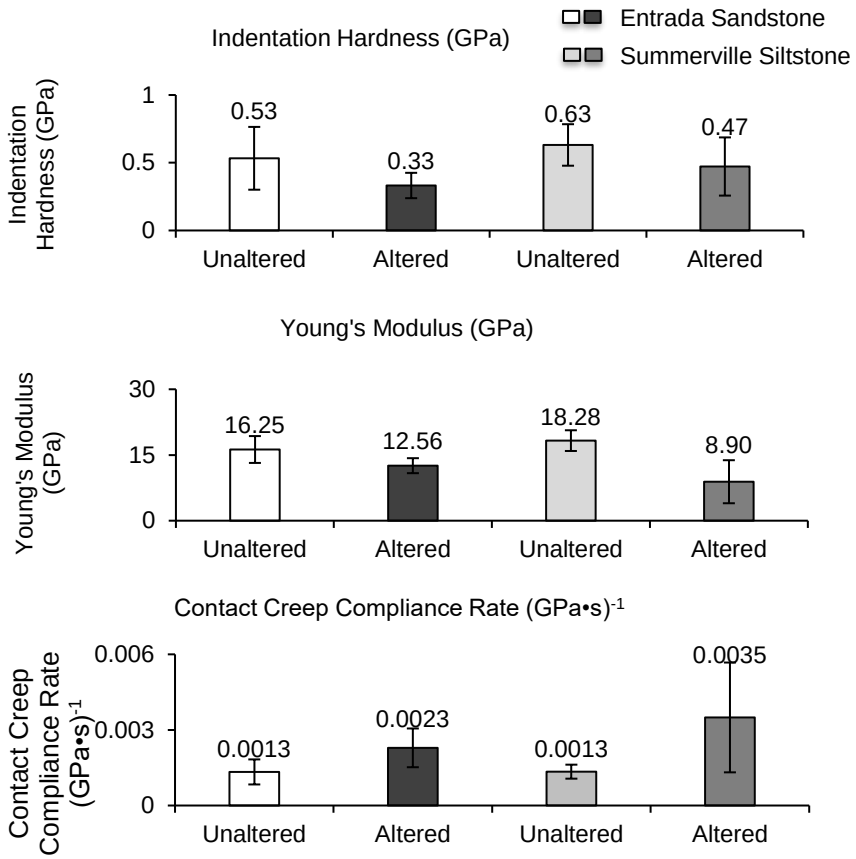

Figure 4.2: Indentation results for (top) indentation hardness, (middle) Young's Modulus, and (bottom) contact creep compliance rate. Error bars represent 95% confidence intervals.

4.3 DISCUSSION

In indentation tests the ratio $A_c/(d_{50})^2$ varies from 1 to 10 in the tested sandstone and from 18 to 100 in siltstone. Hence, it is likely that the indentation test measurements may fluctuate due to grain scale heterogeneity. Indentation loading curves in sandstone

(Figure 4.1b,d) were more irregular than in siltstone. Higher preset load would have been desirable to test a larger volume in sandstone. Indentation in siltstone did not suffer from fluctuations due to lower internal length scales. However, it seems that two indentation tests, characterized by relatively large maximum indentation depths in Figure 4.1c, landed on soft spots. It is uncertain whether these soft spots are the result of CO_2 alteration or not. The exclusion of these measurements reduces the change in contact creep compliance rate from unaltered to CO_2-altered Summerville siltstone from 160% to 70%. Table 4.1 summarizes the parameters measured from the two types of tests including mean values, 95% confidence intervals, and percentage changes after alteration.

Table 4.1: Summary of average results and 95% confidence intervals from micromechanical tests and relative change of mechanical properties after being altered by CO_2-acidified water

	Material	Indentation Hardness (GPa)	Young's Modulus (GPa)	Contact Creep Compliance Rate (1/(GPa·s))
Entrada Sandstone	Unaltered	0.53 ± 0.23	16.25 ± 3.07	0.0013 ± 0.0005
	CO_2-Altered	0.33 ± 0.09	12.56 ± 1.71	0.0023 ± 0.0008
	Change	-38%	-23%	72%
Summerville Siltstone	Unaltered	0.63 ± 0.15	18.28 ± 2.37	0.0013 ± 0.0003
	CO_2-Altered	0.47 ± 0.21	8.90 ± 4.91	0.0035 ± 0.0022
	Change	-25%	-51%	160%

4.3.1 Effect of CO_2 alteration on mechanical parameters

Indentation tests show that average indentation hardness of Entrada sandstone decreased by 38% while that of Summerville siltstone decreased by 25% after CO_2 alteration as shown in Table 4.1. Young's modulus of the Entrada sandstone decreased by 23% while that of siltstone decreased by 51% by CO_2 alteration. Both sandstone and siltstone became more susceptible to time-dependent deformation under influence of stress,

as the contact creep compliance rate increased by 72% for sandstone and 160% for siltstone. A larger measurement volume is needed to reduce variance in the measurement of the contact creep compliance rate for CO_2-altered Summerville siltstone and to better determine where the measured parameter is indicative of CO_2-related weakening and/or a time-dependent response to stress. In general, the indentations on altered siltstone all have less steep unloading curves than the unaltered siltstone, indicating a less stiff material response.

Petrographical analysis shows that the CO_2 altered rocks at Crystal Geyser underwent changes in carbonate content, illite formation, and iron cement dissolution (Wigley et al., 2012; Major et al., 2014) and may explain the apparent weakening indicated by indentation test results.

5. CO_2-Alteration of Crystal Geyser Rocks in the Laboratory

5.1 METHODOLOGY

We altered intact rock samples of Entrada sandstone and Summerville siltstone in a Parr 4563 reactor composed Hastelloy C276 at pressure and temperature setpoints of 9.3 MPa and 80°C. A schematic of the pressure vessel is shown in Figure 5.1. Rock samples were secured in a pressure vessel such that they were immersed in the water phase for the duration of the experiment, accounting for extraction of sampling volumes. Rock samples with a mass of approximately 5 g were immersed in 450 mL of fluid. Samples were altered with either deionized (DI) water or a synthetic brine representative of the groundwater at the Crystal Geyser site, based on the compilation of groundwater chemistry for the Green River Formation (Wanty et al., 1991). Table 5.1Table 5.1 details initial brine composition. CO_2 was added to the pressure vessel through a compressed gas cylinder and a pressure booster and sealed off once the pressure setpoint was attained. The pressure stabilized at the setpoint at approximately 2 hours after the commencement of the experiment. The pressure vessel fluid was mixed with a magnetic stirring rotor at periodic intervals. Experiments ran for durations of one to two weeks. In the cases of DI-water, the selected experiment duration was limited by apparently high mineral dissolution rates that would result in unsuitability for mechanical testing of samples altered in more extended periods. For instance, a one month experiment with DI water and Entrada sandstone resulted in disintegration of the sample.

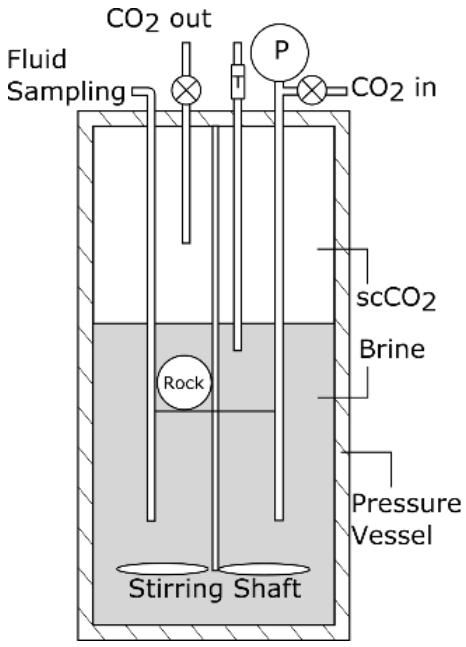

Figure 5.1: Schematic drawings of the utilized pressure reactor

Additional experiments were conducted with powdered rock samples immersed in the aforementioned synthetic brine in order to gain insight into the mechanisms and kinetics of the CO_2-alteration. Rock samples were crushed with a SPEX Sample Prep Shatter Box 8530 and filtered through a 75 μm sieve, and combined with the synthetic brine into a slurry with 25 g of powdered rock per 250 mL of brine. The slurry was added to a Parr 4575 reactor composed of Hastelloy C276 and altered with CO_2 at a pressure of 10 MPa and temperature of 80°C. A magnetic stirring rod was used within the pressure vessel to mix the slurry at 100 RPM for the duration of the experiment.

Table 5.1: Initial synthetic brine compositions. The initial pH of the brine was 7.1.

Compound		
Na^+	24200	mg/L
K^+	1	mg/L
Mg^{2+}	315	mg/L
Ca^{2+}	1455	mg/L
Cl^-	37950	mg/L
HCO_3^-	762.5	mg/L
SO_4^{2-}	3250	mg/L
$SiO_2(aq)$	6	mg/L

I collected slurry samples through a sampling valve at intervals of 3 hours, 24 hours, 48 hours, 1 week and 2 weeks of reaction, such that the liquid to solid ratio stayed constant during the experiment. Prior to sampling, the slurry was mixed thoroughly with a magnetic stirring rod within the pressure vessel at 300 RPM for several minutes. The slurry was centrifuged to separate aqueous and solid samples. Aqueous samples were filtered using a 0.2 μm filter (Whatman). Samples were diluted with de-ionized water and acidified to 1% nitric acid with ultrapure 6N HNO_3 for the ion chromatography (IC) cation analysis and inductively coupled plasma mass spectrometry (ICP-MS) analysis. Non-acidified samples were used for the IC anion analysis. Synthetic brine samples collected prior to the mixing with the powdered samples were taken at the start of each experiment. Aqueous sample processing was the same for both powdered and core alteration experiments. A 2-week blank run was conducted with brine and CO_2 in the absence of a rock sample in order to analyze potential leaching from the Hastelloy reactor used for the core alteration experiments. ICP-MS results demonstrated the presence of minor leaching ranging between 2 to 10 ppm of Ni, Fe, Al, and Zn in the Parr 4563 reactor used for the core

alteration experiments. The Parr 4575 reactor used for the powdered rock alteration experiments demonstrated negligible leaching during a blank run.

5.1.1 Data Analysis

The linear variable differential transformer used to measure the horizontal position was calibrated with a parallel micrometer. In order to obtain the frictional load on the sample surface, the XY-stage spring load contribution was calibrated linearly with horizontal position and subtracted from the measured load.

In order to calculate the scratch width with position along the scratch axis for use in Equations 2.1 and 2.2, the residual failure surfaces of each scratch were imaged with a stereoscopic microscope while a low-angle light was shined along the sample surface in directions perpendicular to scratch travel. The resulting shadow cast on the residual scratch surface facilitates image processing (through MatLab Image Processing Toolbox; see Appendix B) using edge detection to determine the width of the scratch (see Figure B.1). In samples where the surface was substantially rough, grain sizes were large, or substantial brittle chipping apparently occurred, user input was required in tracing the damaged zone. Scratch widths measured using this technique took into account the regions damaged by apparent brittle chipping, which may have extended beyond the contact area of the stylus. A measure of the depth of the scratch with distance along the scratch path is necessary for calculation of the scratch toughness. In order to determine this parameter, the indenter shape function was estimated according to a geometrical transformation of the stylus's conical-spherical shape. This method assumes that any potential blunting of the stylus tip

is negligible, and avoids the necessity of estimating the compliance of the apparatus as the measurement of the scratch depth is made from the residuals of the scratch.

We compute scratch toughness and hardness point by point along the scratch path, and take the average value of the parameters along the path to represent the overall scratch hardness and toughness of the rock sample.

5.1.2 Aqueous Sample Analysis

Filtered aqueous samples from the autoclave alteration experiments were diluted at 15000x and 1500x in a 2% ultrapure nitric acid solution in order to reduce analyte concentrations below approximately 500 ppm. ICP-MS data was acquired using a NexION 350D mass spectrometer (Perkin Elmer) equipped with a collision reaction cell. Testing for sodium, calcium, silica, potassium, and magnesium was done using standard mode; iron, sulfur, silica, and titanium was done using kinetic energy discrimination mode; aluminum was done using dynamic reaction cell mode.

Ion chromatography was used to measure anion and cation concentrations in the aqueous samples. Samples intended for anion analysis were diluted 1000x. Samples intended for cation analyses were initially diluted 3x and acidified with ultrapure 6N HNO_3, and subsequently diluted 1000x with de-ionized water. Samples were analyzed for fluoride, chloride, nitrite, bromide, nitrate, phosphate, and sulfate using a ICS-1100 chromatographer and AS-23 column (Dionex). Calibration standards were prepared with concentrations ranging from 1 mg/L to 100 mg/L. Peaks were identified using Chromeleon (Dionex) software and verified visually.

Analytical errors were measured taking into account dilution error and relative standard deviations of the duplicate sample and standard analysis. The calibration error of the IC measurements was calculated as the standard error of an interpolated value (Salter, 2000). Due to the use of multiple stage dilutions, dilution error is the highest source of error in our analysis.

Initial solid powdered samples and final autoclave-altered samples were analyzed for specific surface area using the Burnauer-Emmett-Teller (BET) nitrogen adsorption method. The measured surface areas were used as one of the input parameters in the geochemical modeling.

5.2 RESULTS

Scratch tests were first conducted on Entrada sandstone and Summerville siltstone samples, including both unaltered and geologically altered rock. Figure 5.2 shows stereoscopic images of the samples after scratching, including samples unaltered, geologically altered and altered with synthetic brine.

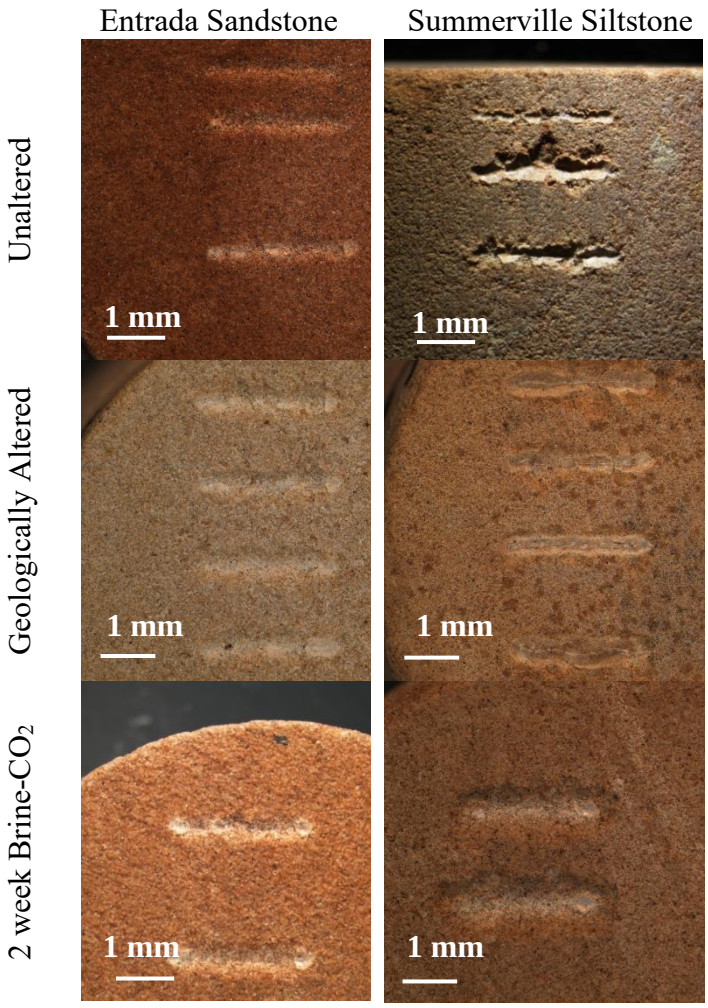

Figure 5.2: Stereoscopic images of unaltered, geologically altered, and 2 week brine-CO_2 altered Entrada sandstone and Summerville siltstone.

The results, shown in Figure 5.3, are in agreement with trends of dual-torsion and short rod testing methodology for calculating the fracture toughness (Major et al., 2014), and suggest a weakening of both rocks due to geological alteration by CO_2.

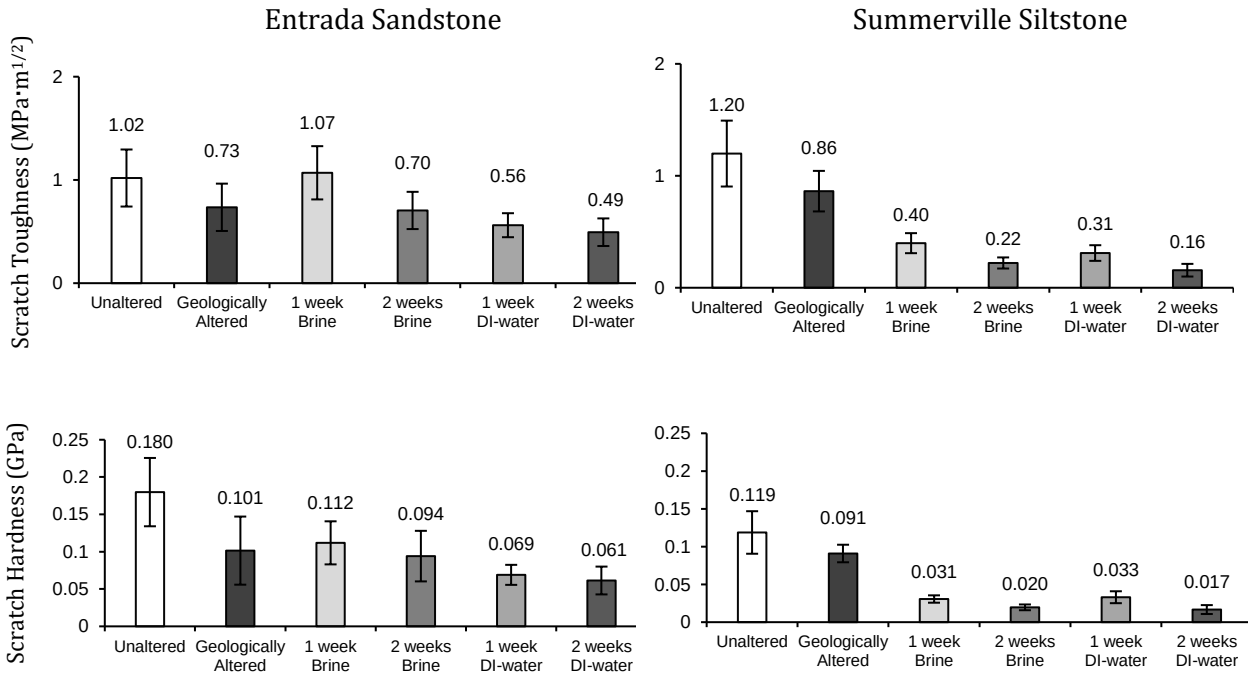

Figure 5.3: Scratch toughness and hardness for Entrada sandstone and Summerville siltstone. All scratch tests were conducted under a 30 N load. Error bars represent one standard deviation over a 5mm scratch length.

The results for samples altered under laboratory conditions are also plotted in Fig. 4. CO_2-DI-water alteration experiments resulted in a severe decrease in scratch toughness for Entrada sandstone, with significant visual alteration in the form of preferential dissolution and cracking. The scratch toughness for Entrada sandstone decreased by 52% after one week of alteration with DI-water and CO_2 whereas scratch hardness decreased by

33%. Alteration with synthetic brine and CO_2 resulted in less severe decreases of scratch toughness of 16% and scratch hardness of 33% after one week.

Decreases in scratch toughness for the laboratory-altered samples of Summerville siltstone reflected substantial weakening, as shown in Figure 5.3. Results indicate relative decreases of 83% in scratch toughness and 89% in scratch hardness after one week for synthetic brine reaction conditions compared to unreacted samples. Similar alteration occurred for the samples altered by CO_2-charged DI water, with uncertainty masking the relative decrease of scratch toughness compared to the brine-altered samples.

5.2.1 Aqueous Chemistry

Results show increased concentrations of lithium, potassium, magnesium, calcium and silicon in the powdered rock alteration experiments. The extent of release for silicon and calcium is higher in the reactors with supercritical CO_2, when compared to the control reactor (no CO_2) for Entrada sandstone and Summerville siltstone (). Other elements (e.g., magnesium, potassium and lithium) are released to the same degree in the control and CO_2 alteration experiments. A compilation of the aqueous chemistry data collected in our experiments for the blank runs, core and powdered rock experiments are tabulated in Appendix A. The mineral dissolution reactions detected in these experiments are the dissolution of calcite and silicate cements (Reactions 5.1 and 5.2):

$$CaCO_3(s) + H^+ \rightarrow Ca^{2+} + HCO_3^- , \quad (5.1)$$

$$SiO_2(am) + H_2O \rightarrow H_4SiO_4\ (aq). \quad (5.2)$$

Blank runs were conducted to test for leaching of metals from the Hastelloy pressure vessel used for the intact core experiments. We detected iron (4.9 ppm), zinc (2.2 ppm), and Ni (1.6 ppm) leaching from the Hastelloy reactor, which was attributed to the use of a stainless steel sample holder inside the vessel. The alteration of powdered samples was conducted in a separate reactor without the use of a stainless steel sample holder, and therefore no iron, zinc, and nickel were released from this reactor during the experiments.

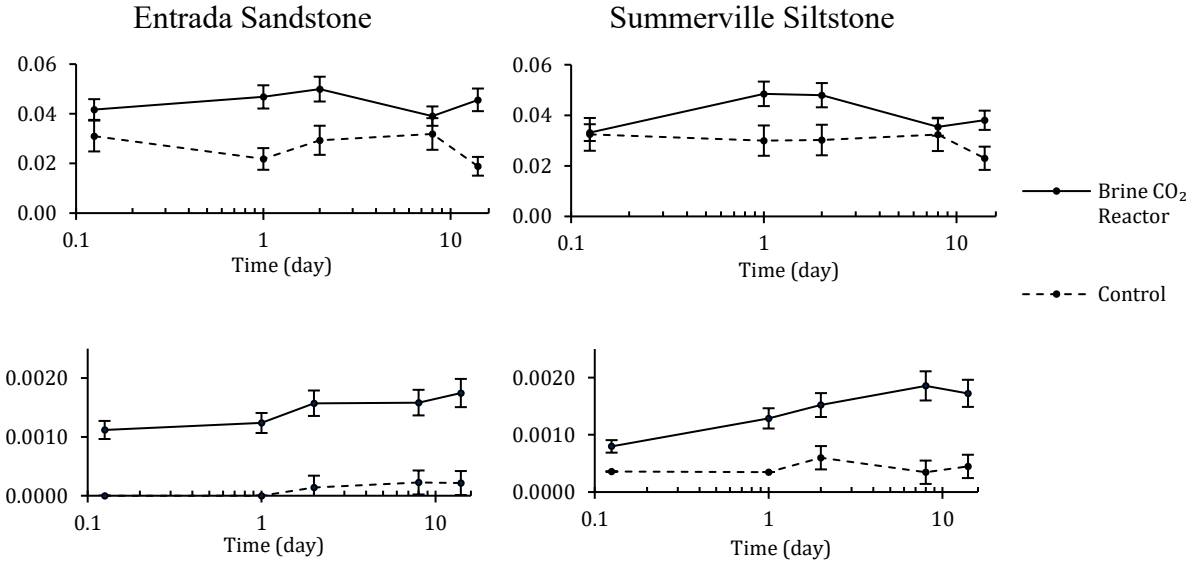

Figure 5.4: Ion mobility trends for aqueous solutions from CO_2-brine alteration experiments with Entrada sandstone and Summerville siltstone powdered samples

5.3 DISCUSSION

5.3.1 Uncertainties in Scratch Test Analysis

In order to reduce uncertainties in measurement of the scratch toughness, it is necessary to capture the indenter shape function through the testing of a known reference material (Akono et al., 2012). The shape function for the indenter was approximated using a simple geometrical transformation that did not take into account variation of the indenter shape function with depth, including contributions from blunting of the diamond tip and apparatus compliance. Ignoring these factors adds uncertainty to the data, which is only marginal compared to the uncertainties in the analysis from the surface roughness and image analysis of the scratch residuals.

As the scratch test may induce localized plastic deformation at small penetration depths, it is necessary to verify if failure in front of the scratch tip occurs in the brittle regime. This problem may be solved through using an instrumented indenter that allows feedback control of scratch depth and vertical load, and conducting a ramping load scratch while simultaneously measuring the scratch toughness. At a certain depth characteristic for each individual material, the calculated scratch toughness may reach an asymptotic value that represents the true fracture toughness of the material (Akono et al., 2012). Due to the limitations of the apparatus used in this thesis, this technique was simplified through the imposing of several scratches at different loads on each unaltered sample. Average scratch toughness was found to vary for each sample up to 30 N normal force, after which the scratch toughness was relatively constant with increasing load, taking into account errors in the analysis. This characteristic threshold load was assumed not to vary after exposure

to CO_2-charged brines, such that the scratch test procedure for post-alteration samples only needed to be tested with loads higher than the original characteristic load.

Both of the methods for the calculation of scratch toughness and hardness used in this study involve the measurement of the scratch width residuals. This study determines scratch toughness through a geometrical transformation that involves the calculation of the indenter shape function from the scratch width (Section 2.2.1). As a result, the values of scratch hardness and toughness have some dependence on one another. An apparatus capable of measuring the depth of the indenter stylus during the scratch test would allow independent calculation of the scratch hardness and toughness.

Variations of surface roughness of the altered samples added uncertainty to the calculations for scratch toughness and hardness. Summerville siltstone cores altered with DI-water exhibited substantial preferential dissolution resulting in localized pitting. The samples were analyzed under an optical microscope, and the scratch test region was selected to minimize the influence of surface roughness. The suitability of the scratch test for testing rock samples after chemical alteration is limited to experiments in which the surface roughness of the material is not substantially changed.

The mechanical parameters determined at an individual point along the scratch path have some uncertainty given that brittle failure events may occur during scratching and fractures may propagate at a characteristic distance from the stylus tip. This uncertainty is no longer significant when the scratch toughness is averaged along the scratch path, accounting for heterogeneities within the rock surface. Future implementations of the scratch toughness measurements should take into account the mismatch of transverse force and width measurements due to fracture propagation ahead of the stylus tip.

5.3.2 Geochemical Observations

Chemical observations for the Entrada sandstone and Summerville siltstone alteration experiments are in agreement with the previously proposed mechanisms of CO_2-induced diagenesis in which rapidly dissolving carbonate phases are followed by more inert silicate phases (Major et al., 2014, Kampman et al., 2016). In the Entrada sandstone, field studies have also shown evidence for mineral re-precipitation, namely high flux fluid pathways having secondary calcite and iron-oxide precipitation closer to the ground surface (where CO_2 exsolves from the brine) (Wigley et al., 2012, Bakker et al., 2016). Low levels of iron were detected in some of the aqueous samples collected from the rock core alteration experiment for both the brine-altered Entrada sandstone and Summerville siltstone, indicating potential dissolution of trace levels of hematite cement. Since I found that some iron was leaching from the stainless steel sample holder used for the alteration of rock cores, it is not feasible to distinguish iron from hematite dissolution and iron leaching from the reactor for these samples (Appendix A). The extent of mineral dissolution in the intact rock core alteration experiments was relatively low, due to the low reactive surface area and kinetic constrains on mineral dissolution. Therefore, the resulting concentrations of ions in the reacting fluids were below the detection limit of our analytical methods. Increased reactive surface area for the powdered samples (11.4 m^2/g for Summerville siltstone, and 10.7 m^2/g for the Entrada sandstone prior to the alteration experiment, based on BET analysis (Aman et al., submitted)) allowed for measurable calcium, lithium, potassium, magnesium, and silicon release on the timescale of this experiment. Additionally, based on the X-ray microtomography imaging and analysis (Section 5.3.3), the mass of the core sample altered is estimated at ~3 g in comparison to

the 25 g samples used in the powdered experiments. Calcium and silicon concentrations were systematically different when CO_2 and control (no CO_2) powdered rock alteration experiments are compared, while other released elements (magnesium, lithium, and potassium) were similar in the control and CO_2 reactors. The results of geochemical modeling of powder sample reactions with the same synthetic brine used in the autoclave experiments for Entrada sandstone and Summerville siltstone are shown in Figure 5.5 (Aman et al., submitted). The model predicts higher calcium release for the CO_2 reactor experiments, compared to the control reactor experiments, as well as calcium concentrations consistent with my observations. The release of silicon, predicted based on the mineral composition of the sample (Table 2.1), and mineral dissolution kinetics (Table 5.2), underestimates the aqueous concentration of silicon for the CO_2 reactor experiment compared to the observed concentrations. We hypothesize that this is due to the likely presence of poorly-crystalline silicate-containing cement on the surfaces of the grains, with a relatively higher rate of dissolution (compared to other silicates, e.g. quartz and albite).

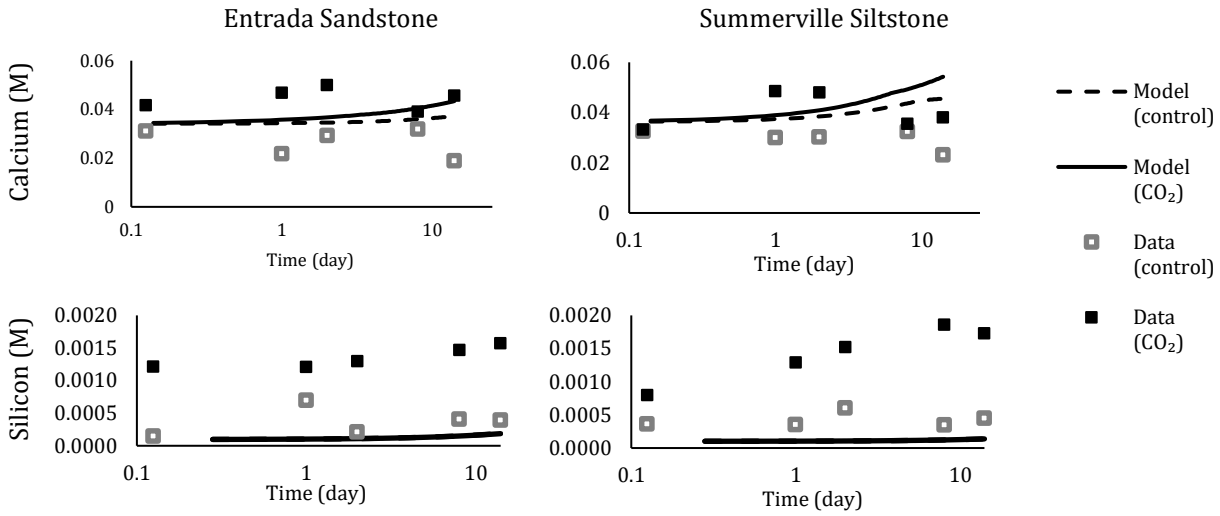

Figure 5.5. Geochemical modeling (lines) and observations (points) for Entrada sandstone (left) and Summerville siltstone (right) (Aman et al., submitted).

The surface area of the powdered samples was measured before and after the 2-week alteration experiment. The surface area prior to the alteration was 11.4 m^2/g for Summerville siltstone, and 10.7 m^2/g for the Entrada sandstone. After the alteration experiment, surface area for both samples increased in both the CO_2 and control experiments, and became 19.3 m^2/g (CO_2) and 15.6 m^2/g (control) for Entrada sandstone, and 16.3 m^2/g (CO_2) and 14.7 m^2/g (control) for Summerville siltstone. For both rocks, the increase in the reactive surface area is larger for the CO_2 reactor experiments, indicating a higher degree of chemical alteration, consistent with the aqueous chemistry observations.

Table 5.2: Mineral dissolution weight percentage and rate used in the geochemical models.

Mineral	Weight %	Kinetic rate constant log (mol cm^{-2} sec^{-1})
Quartz	46	-16
Calcite	9	-10
Illite	10	-13
Smectite	11	-13
Dolomite	9	-10
Kaolinite	6	-13
Orthoclase	4	-14
Albite	2	-15

In summary, the geochemical modeling and aqueous chemistry observations indicate dissolution of calcite and silicate cements on the timescale of my laboratory experiments ~2 weeks. Aman et al. documented that the degree of chemical alteration is more pronounced in the CO_2 systems compared to the control systems with brine only (no added CO_2).

5.3.3 Dissolution Front Observations

CO_2-induced mineral dissolution was confirmed through X-ray microtomography. I measured a reaction front zone on the order of 1 mm thick on the outer surfaces of cores reacted with DI-water and brine (Figure 5.6). The reaction zone in the images appears as a darker region on the outer surface of the samples. The images have been corrected for beam hardening, such that the variations in shade represent the X-ray absorption properties of the material. Scratch residuals shown in the Summerville siltstone sample correspond to

top-down views in Figure 5.2. This region is characterized by an increase in porosity with respect to the original core. As discussed above, due to the limited extent of reaction and relatively large fluid volumes, the resulting aqueous concentrations of constituents released from the mineral dissolution was below the limit of detection for our analytical techniques. Scratch residuals shown in Figure 5.6 on an Entrada sandstone core reacted with synthetic brine and CO_2 penetrate approximately 350 μm of the overall reaction zone, confirming the scratch test's ability to probe the reacted skin on the rock cores. Similarly, residuals shown in Figure 5.6 on a Summerville siltstone core reacted with synthetic brine and CO_2 cover the complete depth of the reaction front zone (700 μm).

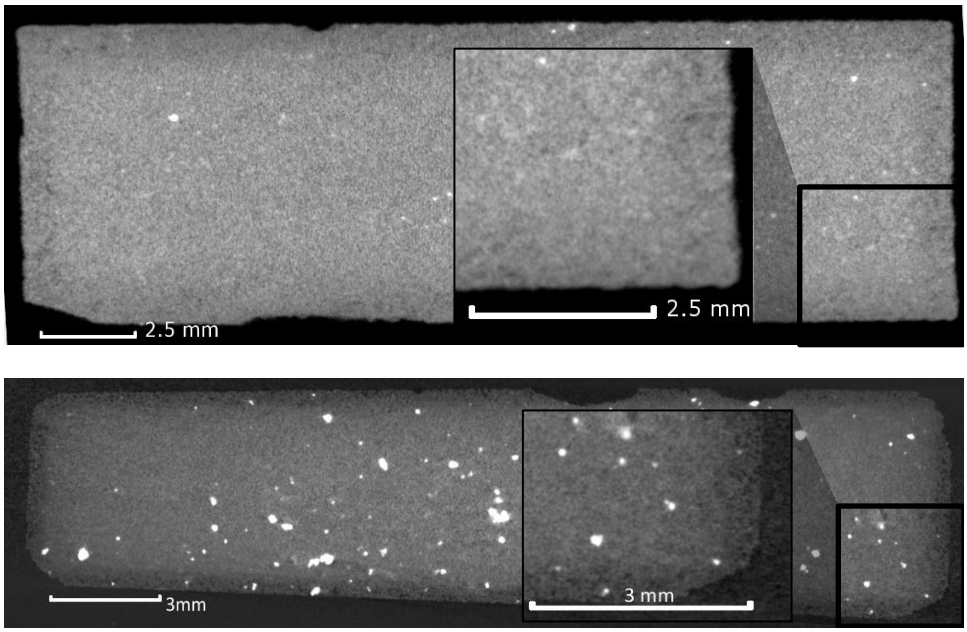

Figure 5.6: μCT images of Entrada sandstone (top) and Summerville siltstone (bottom) after 2 week alteration with synthetic brine. Periphery darker regions indicate higher porosity.

With the scratch test successfully probing the reacted region, the mechanisms of chemical alteration causing the degradation of scratch toughness and hardness can be inferred from the chemical alteration observations recorded for the powdered core samples. Similar mineral dissolution trends are expected between the intact core and powdered experiments, but differing reactive surface areas have to be taken into account. We conclude that the degradation of mechanical properties in the Entrada sandstone and Summerville siltstone on the time scale of our laboratory experiments is primarily due to the dissolution of carbonate cement and minor amounts of silicate cement. Longer (tens, hundreds, and thousands of years) periods of alteration are not feasible for laboratory tests, and may show alternative mechanisms for further decrease or increase of the reservoir rock strength.

6. Conclusions

CO_2 injection into geological formations disturbs the geochemical equilibrium such that some mineral phases may dissolve with an ensuing change of geomechanical properties of the host formations.

I tested the suitability of micromechanical tests to give insight into changes of mechanical properties with and without CO_2-induced geochemical alteration. These kinds of tests are cost-efficient, repeatable, and are successful in quantifying the degree of mechanical degradation of rock cores altered in an pressure reactor with limited (~1 mm) reaction front thicknesses. Interaction volumes for the scratch test can be managed such that only the reacted region is tested while the unreacted core of the sample does not contribute to the measurement of mechanical properties.

Entrada sandstone and Summerville siltstone show degradation of fracture toughness and hardness with increasing duration of exposure to CO_2-charged brines in both laboratory experiments and natural analogues. Mechanical alteration as evidenced by micromechanical tests is more severe in laboratory-altered samples in comparison to geologically altered field samples. Higher solid to liquid ratios were used in the laboratory experiments than are typical of natural systems. An ensuing reduction of carbonate saturation and re-precipitation of carbonate cement would differentiate the reactions and the geomechanical changes observed in the laboratory experiments from those expected in the field.

At the Crystal Geyser site near Green River, Utah, diagenesis of Entrada sandstone and Summerville siltstone resulted in rapid dissolution of carbonate followed by less reactive silicate phases. In the laboratory study, I primarily observed dissolution of calcite

and minor amounts of silicate cements. Geologically altered samples exhibit lower amounts of carbonates, suggesting carbonate dissolution, but with regions of calcite re-precipitation. During the pressure reactor experiments presented in this study, the dissolution of calcite and silicate cements is inferred as the primary mechanism of the degradation of Entrada sandstone and Summerville siltstone samples with CO_2-alteration. Alternative mechanisms may lead to further weakening or strengthening at tens, hundreds and thousands of years of alteration.

Potential implications of dissolution under *in situ* stress and subsequent degradation of mechanical properties include modification of yield stress locus, reactivation and propagation of natural fractures, caprock straining, and chemo-mechanical induced seismicity. The unstressed reaction experiments conducted in this study suggest that CO_2-related alteration of the rock fabric may result in increases of porosity and therefore its transport properties. Reductions in scratch toughness and hardness are representative of overall reductions of resistance to fracture, shear strength and compressive yield stresses. In reservoirs where the *in situ* stress state is close to the yield stress, CO_2-promoted alteration may be significant enough to induce reservoir rock deformations, leading to caprock straining or horizontal stress relaxation. Decreases in fracture toughness may result in the reactivation and propagation of natural fractures, creating potential high permeability channels. Injection of fluid into a reservoir can alter the stress-state and induce fault reactivation. Many faults are already close to a state of critical equilibrium between formation fluid pressures and *in situ* stresses, in which small perturbations can induce fault slip. Micromechanical testing is an efficient method to investigate the susceptibility of reservoir rocks to these emergent behaviors from coupled chemo-mechanical processes.

6.1 RECOMMENDATIONS

Micromechanical tests ought to account for the internal length scales of heterogeneous geological materials. Conducted tests target a tested volume that was large enough to capture the response of the cemented rock matrix rather than the individual properties of mineral grains. Results could be improved upon by increasing the fidelity of the experimental setup and sample preparation scheme. Specifically, implementation of load and displacement controlled vertical load actuation would allow more accurate calculation of the indenter displacement function and material internal length scales, allowing better estimates of uncertainty.

The autoclave experiments designed here have the potential to better represent real geochemical processes through more robust experiment design. A main limitation to the application of the results to interpretation of field scale processes is the differences in fluid to rock ratios between the laboratory and field. An experiment that reduced that discrepancy by reducing fluid availability and increasing experiment duration may represent field processes more accurately.

Appendix A: Aqueous Solution Concentrations from CO_2-Brine Alteration Experiments

Table A.1: Aqueous solution concentrations from CO_2-brine alteration experiments

			Concentration (M)								
			Ion Chromatography (IC)						Inductively Coupled Plasma-Mass Spectrometry (ICP-MS)		
	Time (days)	pH	Chloride	Sulfate	Na	K	Mg	Ca	Ca 40	Mg	Si
Entrada sandstone powder (control)	0	7.16	0.95	0.030	1.030	0.0001	0.015	0.033	0.026	0.009	0.0000
	0.125	7.05	0.98	0.031	0.993	0.007	0.016	0.031	0.021	0.009	BDL*
	1	7.1	0.83	0.026	0.667	0.005	0.012	0.022	0.023	0.010	BDL*
	2	7.22	0.94	0.030	0.945	0.007	0.016	0.029	0.021	0.009	0.0001
	8	7.45	1.00	0.031	1.004	0.008	0.017	0.032	0.027	0.013	0.0002
	14	7.45	0.96	0.032	0.576	0.004	0.011	0.019	0.024	0.010	0.0002
Entrada sandstone powder (CO_2)	0	7.1	0.95	0.030	1.030	0.0001	0.015	0.033	0.026	0.009	0.0002
	0.125	6.22	0.98	0.031	0.870	0.006	0.016	0.042	0.037	0.010	0.001
	1	6.22	0.97	0.032	0.872	0.007	0.016	0.047	0.037	0.010	0.001
	2	6.16	0.89	0.029	0.929	0.007	0.018	0.050	0.042	0.012	0.002
	8	6.2	0.83	0.026	0.732	0.005	0.015	0.039	0.037	0.010	0.002
	14	6.35	0.79	0.025	0.940	0.007	0.018	0.046	0.037	0.011	0.002
Maximum Relative Error			0.14	0.05		0.04		0.04	0.04	0.29	0.14

*BDL: Below detection limit

Table A.1 Continued

	Time (days)	Concentration (M)									
		IC					ICP-MS				
		Chloride	Sulfate	Na	Mg	Ca	Mg	K	Si	Fe	Al
	0.125	1.13	0.033	0.89	0.010	0.025	0.008	0.0001	0.0004	0.0000	0.0002
Entrada sandstone	1	0.70	0.024	0.79	0.009	0.023	0.007	0.0002	0.0003	0.0001	0.0002
core (CO_2)	4	1.10	0.033	0.91	0.010	0.028	0.010	0.0003	0.0005	0.0001	0.0003
	8	0.42	0.014	0.87	0.010	0.028	0.009	0.0002	0.0003	0.0001	0.0002
	14	0.68	0.024	0.96	0.011	0.032	0.010	0.0003	0.0003	0.0002	0.0002
Maximum Relative Error		0.10	0.05	0.04	0.04	0.04	0.17	0.19	0.19	0.19	0.14

Table A.1 Continued

	Time (days)	pH	Concentration (M)							
			IC						ICP-MS	
			Chloride	Sulfate	Na	K	Mg	Ca	Mg	Si
Summerville siltstone powder (control)	0	7.16	0.89	0.028	0.929	0.0003	0.013	0.028	0.013	0.0003
	0.125	7.05	1.03	0.031	1.059	0.004	0.016	0.032	0.013	0.0004
	1	7.1	0.68	0.021	0.984	0.004	0.015	0.030	0.010	0.0004
	2	7.22	1.04	0.030	0.992	0.005	0.015	0.030	0.012	0.0006
	8	7.45	1.04	0.031	1.057	0.004	0.015	0.032	0.010	0.0003
	14	7.45	0.603	0.019	0.739	0.003	0.011	0.023	0.010	0.0004
Summerville siltstone powder (CO_2)	0	7.16	0.89	0.028	0.92	0.000	0.013	0.028	0.013	0.0003
	0.125	6.22	1.03	0.031	0.83	BDL	0.011	0.033	0.012	0.0008
	1	6.22	1.05	0.029	0.96	0.004	0.016	0.048	0.013	0.0013
	2	6.16	0.93	0.027	1.07	BDL	0.018	0.048	0.014	0.0015
	8	6.2	0.95	0.025	0.82	BDL	0.015	0.035	0.015	0.0019
	14	6.35	1.08	0.027	1.18	0.005	0.020	0.038	0.015	0.0017
Maximum Relative Error			0.11	0.05	0.06	n/a	0.04	0.07	0.14	0.15

Table A.1 Continued

	Time (days)	Concentration (M) IC Chloride	Sulfate	Na	Mg	Ca	ICP-MS Mg	K	Si	Fe	Al
	0	0.85	0.029	0.68	0.007	0.017	0.009	0.0001	0.0004	0.00001	0.0002
Summerville siltstone core (CO_2)	0.125	0.48	0.017	0.76	0.007	0.020	0.009	0.0001	0.0004	0.00001	0.0002
	1	1.18	0.037	0.92	0.010	0.030	0.009	0.0002	0.0004	0.00002	0.0002
	4	1.09	0.035	0.69	0.007	0.024	0.007	0.0001	0.0003	0.00002	0.0002
	7	1.12	0.035	0.55	0.005	0.019	0.005	0.0001	0.0002	0.00001	0.0001
	14	0.85	0.029	1.08	0.012	0.044	0.009				
Maximum Relative Error		0.10	0.05	0.04	0.04	0.04	0.17	0.19	0.17	0.19	0.14

	Time (days)	Concentration (M) ICP-MS Ni	Fe	Zn	Al
Blank Run*	0.125	0.68	0.056	0.31	0.009
	1	0.42	0.041	0.28	0.008
	4	0.66	0.056	0.32	0.009

*The blank run was completed with synthetic brine in the reactor used to alter the core samples. A different reactor with no leaching present was used for the powdered samples.

Appendix B: Algorithm to Calculate Scratch Toughness and Hardness via Scratch Testing and Image Analysis

Scratch Data and Image Analysis Script

```
% This script carries out analysis for a scratch test in order to
calculate
% scratch toughness and hardness.

% The code is interactive at certain sections which are marked by
section
% headers (%%)

% Dependencies:
% datamanip.m - Function that accepts a data set of LVDT data
% and load cell data, and outputs frictional load versus scratch
position
% in a matrix. kIC.m - Function that calculates the scratch toughness
and
% hardness for an input of frictional load versus scratch position.
% magicwand.m - By Daniel Lau, accessed 02/16. Available at Matlab File
% Exchange: https://www.mathworks.com/matlabcentral/fileexchange/130
% export_fig.m - By Yair Altman, accessed 02/16. Available at Matlab
File
% Exchange: https://www.mathworks.com/matlabcentral/fileexchange/23629
% cutsamples.m - By Aslak Grinsted, accessed 02/16. Available at Matlab
% File Exchange:
https://www.mathworks.com/matlabcentral/fileexchange/3447
% units.m - By Rob deCarvalho, accessed 02/16. Available at Matlab File
% Exchange: https://www.mathworks.com/matlabcentral/fileexchange/9873
% peakfinder.m - By Nathanael Yoder, accessed 02/16. Available at
Matlab
% File Exchange:
https://www.mathworks.com/matlabcentral/fileexchange/25500

% Steps for running the code:

% 1. Run the complete code once after saving to a new file. Terminate
the
% code after running it; the code does not need to complete.

% 2. Run individual sections of the code, starting with Section 2.
Follow
```

```
% any instructions in the comments. Sections can generally be run
multiple
% times

% Initialization
clc;  % Clear the command window.
clear % Clear variables
workspace;  % Make sure the workspace panel is showing.
format long g;
format compact;
fontSize= 15;
u=units; %Define unit structure for unit conversion (see units.m for
further info)
mName=mfilename; % Grabs the script title for automatic variable
retrieval
% mName='';

%% 1. Edit lines 45-51
close all;
path='..\Images\ICMB Stereoscope\'; %Path to image folder
%Path to invidual images of the scratches
imagefile='Summerville
Siltstone\161019_summerville_1wkbrine_s1_mag2.jpg';
imagefile2='Summerville
Siltstone\161019_summerville_1wkbrine_s1_mag2_opp.jpg';
name='161014_sumville_1wkbrine_s1_3-17kg'; % Name of LVDT/load data
file
verticalLoad=3.17; % Vertical load used in scratch test in kg
cal=40/11; % Calibration to convert between # of pixels and microns

fullFileName= [path,imagefile];
fullFileName2= [path,imagefile2];
if ~exist(fullFileName, 'file')
    errorMessage= sprintf('Error: %s does not exist in the search path
folders.', fullFileName);
    uiwait(warndlg(errorMessage));
    return;
end
grayImage= imread(fullFileName);
grayImage2= imread(fullFileName2);
%% 2. Select region of interest in image to crop for faster processing
time
[~,rect2]=imcrop(grayImage); clipboard('copy',rect2); close(gcf)
% This section opens up an interactive image; select a region to crop
and
% paste the resulting matrix in lines 67-68
%% 3. Edit lines 67-68 with copied crop coordinates from previous
section
grayImageOrig=imcrop(grayImage,[2.51 388.51 1605.98 810.98]);
```

```
grayImageOrig2=imcrop(grayImage2,[2.51 388.51 1605.98 810.98]);
grayImage= imresize(grayImageOrig,0.2);
grayImage2= imresize(grayImageOrig2,0.2);

% Get the dimensions of the image. numberOfColorBands should be = 1.
[rows, columns, numberOfColorBands]= size(grayImage);
if numberOfColorBands > 1
    % It's not really gray scale like we expected - it's color. Convert
it
    % to gray scale by taking only the green channel.
    grayImage = grayImage(:, :, 2); % Take green channel.
end
[rows2, columns2, numberOfColorBands2]= size(grayImage2);
if numberOfColorBands2 > 1
    grayImage2 = grayImage2(:, :, 2);
end

% Display the original gray scale image.
handle1=figure;
subplot(3, 3, 1);
hgrayImage=imshow(grayImage, []);
axis on;
title('Original Grayscale Image', 'FontSize', fontSize);
subplot(3, 3, 2);
hgrayImage2=imshow(grayImage2, []);
axis on;
title('Opposite Grayscale Image', 'FontSize', fontSize);
% Enlarge figure to full screen.
set(gcf, 'Units', 'Normalized', 'OuterPosition', [0 0 1 1]);
% Give a name to the title bar.
set(gcf, 'Name', 'Image Analysis Steps', 'NumberTitle', 'Off')
drawnow;

% Let's compute and display the histogram.
[pixelCount, grayLevels] = imhist(grayImage);
subplot(3, 3, 3);
bar(grayLevels, pixelCount);
grid on;
title('Histogram of original image', 'FontSize', fontSize);
xlim([0 grayLevels(end)]); % Scale x axis manually.
[pixelCount2, grayLevels2] = imhist(grayImage2);
subplot(3, 3, 6);
bar(grayLevels2, pixelCount2);
grid on;
title('Histogram of opposite image', 'FontSize', fontSize);
xlim([0 grayLevels(end)]); % Scale x axis manually.

% Parse the image into binary based on a certain threshold (recommend
to
```

```
% check values in imageJ or matlab image processing toolbox before
deciding
% on a value)
%% 4.1 Edit line 118 - Select a threshold level
level=20; % Choose a level based on the histogram figure
subplot(3,3,4);
BW = im2bw(grayImage, level/256);
hBW=imshow(BW);
axis on;
title(['Binary Original Image; Theshold ',num2str(level)], 'FontSize',
fontSize);

%% 4.2 Edit line 126 - Select a threshold level
level2=20; % Choose a level based on the histogram figure
h2=subplot(3,3,5);
BW2 = im2bw(grayImage2, level2/256);
hBW2=imshow(BW2);
axis on;
title(['Binary Opposite Image; Theshold ',num2str(level2)], 'FontSize',
fontSize);

%% 5. Edit lines 136-137
% Select x, y coordinates of shaded scratch areas of interest from
% currently displayed subplots 4 & 5 and input in next coordinate
matrices
rgbImage = repmat(255*BW/max(BW(:)),[1 1 3]);
rgbImage2 = repmat(255*BW2/max(BW2(:)),[1 1 3]);
coordMat1=[109,49];
coordMat2=[168,98];
scratch=0;
coSize1=size(coordMat1);
coSize2=size(coordMat2);

%Use magic wand function to select only the scratch area
for i2=1:coSize1(1) % Combine two scratch areas into one image
    scratch=scratch+magicwand(rgbImage, coordMat1(i2,1),
coordMat1(i2,2), 3);
end
for i2=1:coSize2(1)
    scratch=scratch+magicwand(rgbImage2, coordMat2(i2,1),
coordMat2(i2,2), 2);
end
subplot(3,3,7)

%Fill areas inside image to complete scratch region
scratchFill=imfill(scratch,'holes');
imshow(scratchFill)
title('Combination of Trace Sections', 'FontSize', fontSize);
```

```
%Determine indices of upper and bottommost non-zero values in each row
(for
%measuring width of scratch)
subplot(3,3,8)
scratchBound=bwperim(scratchFill); %Plot perimeter of scratch
[row,col]=find(scratchBound); %Get indexes of points in perimeter
matrix
imshow(scratchBound)
scratchBoundResize=imresize(scratchBound,5);
title('Perimeter of Scratch', 'FontSize', fontSize);

ind = zeros(size(col));
minCol=min(col);maxCol=max(col);
lengthScratch=maxCol-minCol; %Determine length of scratch by
subtracting last col coord from first
for i = 1:length(col) %Determine how many points are in each column
    ind(i) = sum(col==col(i));
end
yIndex2=1;
widthMat=zeros(lengthScratch,1);
scratchShape=scratchBound;
for i = 1:lengthScratch
    try
        yIndex1=yIndex2;
        nRows=ind(yIndex2); %# Rows in current column
        yIndex2=yIndex1+nRows;
        % Have indexes, now subtract row at bottom index in each column
        % from top index to determine length of each column
        top=row(yIndex1);
        colCur=col(yIndex1);
        bot=row(yIndex2-1);
        widthMat(i)=bot-top;

        % Plot a filled shape showing final length of scratch for error
        % checking/quality control
        scratchShape(top:bot,col(yIndex1))=1;
    catch
        break
    end
end
subplot(3,3,9)
set(hgrayImage,'AlphaData',1-scratchBound)
set(hgrayImage2,'AlphaData',1-scratchBound)

% Return image back to original size
scratchShape=imresize(scratchShape,5);
imshow(scratchShape)
title('Final Scratch Image for Data Export', 'FontSize', fontSize);
axis on;
```

```
%% 6. Rerun section 6 multiple times
% Comment/uncomment Line 211-212 to switch editing images
% Comment/uncomment Line 219-220 to add or subtract from the image
% selection
handleE=figure;

hgrayImageEdit=imshow(grayImageOrig); %Uncomment either line to choose
which shadow direction to look at
% hgrayImageEdit=imshow(grayImageOrig2);

set(gcf, 'Units', 'Normalized', 'OuterPosition', [0 0 1 1]);
sGrayImageEdit=size(grayImageOrig);
scratchBoundResizeCropped=scratchBoundResize(1:sGrayImageEdit(1),1:sGra
yImageEdit(2));
set(hgrayImageEdit,'AlphaData',1-scratchBoundResizeCropped)

name2='Add'; BWselect2=roipoly; %% Select areas needed for tracing with
mouse, then input outputs next section
% name2='Sub';BWselect2=roipoly; %% Uncomment this line if completing a
% subtraction
BWselect=[];
if ~isempty(BWselect2)
    BWselect=imresize(BWselect2,.2);
end

% load existing SelectedVariables.mat to save user selected points into
field=[mName,name2];
fieldAdd=[mName,'Add'];
fieldSubtract=[mName,'Sub'];
srwitch=0;
if exist('SelectedVariables.mat','file')
    load('SelectedVariables')
else
    SelectedVariables=struct(field,BWselect);
    srwitch=1;
end
% check Sim was indeed loaded and if so extend it
if srwitch==0
    if exist('SelectedVariables','var') && ~isempty(SelectedVariables)
        if isfield(SelectedVariables,field)

            emptyIndex = find(arrayfun(@(SelectedVariables)
isempty(SelectedVariables.(field)),SelectedVariables));
            if ~isempty(emptyIndex)
                SelectedVariables(emptyIndex(1)).(field)=BWselect;
            else
                SelectedVariables(end+1).(field) = BWselect;
```

```
            end
        else
            tmp=cell(size(SelectedVariables));
            [SelectedVariables(:).(field)]=deal(tmp{:});
            SelectedVariables(1).(field) = BWselect;
        end

    else
        % create a new Sim (presumably the first time)
        SelectedVariables(1).(field) = BWselect;
    end
end
% save the extended Sim
try SelectedVariables=rmfield(SelectedVariables,'UserSubtract');
end
save SelectedVariables SelectedVariables

% Add/subtract the current selected masks into the total scratch
selection
%scratch add
scratch2=scratch;
sSelect=size(SelectedVariables,2);
if isfield(SelectedVariables,fieldSubtract)
    for i3=1:sSelect
        if ~isempty(SelectedVariables(i3).(fieldSubtract))
            scratch2=scratch2-SelectedVariables(i3).(fieldSubtract);
        end
    end
end
scratch2(scratch2<0)=0;

if isfield(SelectedVariables,fieldAdd)
    for i3=1:sSelect
        if ~isempty(SelectedVariables(i3).(fieldAdd))
            scratch2=scratch2+SelectedVariables(i3).(fieldAdd);
        end
    end
end
scratch2(scratch2>1)=1;
%scratch subtract

scratch=scratch2;

%Replot data with new trace additions/subtractions
try close(handleE)
end
subplot(3,3,7)
```

```
%Fill areas inside image to complete scratch region
scratchFill=imfill(scratch,'holes');
imshow(scratchFill)
title('Combination of Trace Sections', 'FontSize', fontSize);

%Determine indices of upper and bottommost non-zero values in each row
(for
%measuring width of scratch)
subplot(3,3,8)
scratchBound=bwperim(scratchFill); %Plot perimeter of scratch
[row,col]=find(scratchBound); %Get coordinates of points on perimeter
imshow(scratchBound)
scratchBoundResize=imresize(scratchBound,5);
title('Perimeter of Scratch', 'FontSize', fontSize);

ind = zeros(size(col));
minCol=min(col);maxCol=max(col);
lengthScratch=maxCol-minCol; %Determine length of scratch by
subtracting last col coord from first
for i = 1:length(col) %Determine how many points are in each column
    ind(i) = sum(col==col(i));
end
nRows=0;
yIndex1=1;
yIndex2=1;
widthMat=zeros(lengthScratch,1);
scratchShape=scratchBound;
for i = 1:lengthScratch
    try
        yIndex1=yIndex2;
        nRows=ind(yIndex2); %# Rows in current column
        yIndex2=yIndex1+nRows;
        % Have indexes, now subtract row at bottom index in each column
        % from top index to determine length of each column
        top=row(yIndex1);
        colCur=col(yIndex1);
        bot=row(yIndex2-1);
        widthMat(i)=bot-top;

        % Plot a filled shape showing final length of scratch for error
        % checking/quality control
        scratchShape(top:bot,col(yIndex1))=1;
    catch
        break
    end
end
subplot(3,3,9)
scratchBound2=bwperim(scratchShape); % Grab perimeter of final scratch
shape to plot on original image
```

```
set(hgrayImage,'AlphaData',1-scratchBound)
set(hgrayImage2,'AlphaData',1-scratchBound)

% Return image back to original size
scratchShape=imresize(scratchShape,5);
imshow(scratchShape)
title('Final Scratch Image for Data Export', 'FontSize', fontSize);
axis on;

widCal=widthMat.*5.*cal;
pos=1:lengthScratch;
pos=pos.*5.*cal./1000;
dataIM=horzcat(pos.',widCal);   %data file containing scratch position
(mm) in the 1st column, scratch width (micron) in the right column
dataIM(:,1)=dataIM(:,1).*u.mm; %convert image data to base metric units
for calculations
dataIM(:,2)=dataIM(:,2).*u.um;

% Position is in m, width in m
agiPath=['Agilent DAQ Data\',name,'.csv']; %
load gong, sound(y,1/2*Fs)
%% 7. Edit line 363 according to the below comments
try close('Load/LVDT Processing Steps')
end
[dataDAQ,fighandle]=datamanip_v4(agiPath,1.63,13.5,1/2,1,350,150);
% Increase second input to extend beginning of scratch
% Increase third value to reduce scratch length
% Increase sixth value to increase the distance from the start of the
% scratch to select the initial load for stage load calibration
% Increase seventh value to increase the distance from the start of the
% scratch to select the initial load for stage load calibration

dataDAQ(:,1)=dataDAQ(1,1)-dataDAQ(:,1);     %data file containing
scratch position (mm) in the 1st column, transverse force (N) in the
right column.
dataDAQ(:,1)=dataDAQ(:,1).*u.mm; %convert DAQ data to base metric units
for calculations
dataDAQ(:,2)=dataDAQ(:,2).*u.N;

% Position is in m, load in N.

% Interpolate data to regularly spaced intervals that line up for both
% datasets using cutsamples.m
posDAQ=dataDAQ(:,1);
loadDAQ=dataDAQ(:,2);
posIM=dataIM(:,1);
widthIM=dataIM(:,2);
xDAQsi=(0:.00001:round(posDAQ(end),4))';
```

```
xDAQei=xDAQsi+.00001;
loadInterpTemp=cutsamples(posDAQ,loadDAQ,xDAQei,xDAQsi);
xIMsi=(0:.00001:round(posIM(end),4))';
xIMei=xIMsi+.00001;
widthInterpTemp=cutsamples(posIM,widthIM,xIMei,xIMsi);

load chirp, sound(y,1/2*Fs)
%% 8. Edit/uncomment lines 396-7 for quality control of results
% From the start of widthInterp or loadInterp
widthInterp=widthInterpTemp;
loadInterp=loadInterpTemp;
%# of entries to be removed from start of widthInterp
widthInterp(1:45,:)=[]; switch1=1;
% loadInterp(1:40,:)=[]; switch1=2; %# of entries to be removed from
start
% of loadInterp
xFin=mean([xDAQsi, xDAQei],2);
l1=length(widthInterp);
l2=length(loadInterp);
minLength = min([l1, l2]); % Make sure that columns are of even length
loadInterp(minLength+1:length(loadInterp)) = [];
xFin(minLength+1:length(xFin)) = [];
widthInterp(minLength+1:length(widthInterp)) = [];
%Concatenate data into one matrix
dataFinTemp=horzcat(xFin,loadInterp,widthInterp);
%Remove any rows with NaN entries (these were created by interpolation
%process)
dataFinTemp=dataFinTemp(~any(isnan(dataFinTemp),2),:);

%% 9. Edit/uncomment lines 416-7 for quality control of results
% Correct second term in kIC to appropriate load value. Run code for
% fracture toughness and scratch hardness calculations at each data
point.
dataFin=dataFinTemp;
% dataFin(1:100,:)=[]; % Remove initial point outliers
% dataFin(end-50:end,:)=[]; % Remove end point outliers
[frac,hardness,depth]=kIC(dataFin,verticalLoad);

try close(handle3)
end
pos=dataFin(:,1)./u.mm;
handle3=figure;
plot(pos,frac*1000,pos,hardness*1000,pos,dataFin(:,2)*100,pos,dataFin(:
,3)./u.um)
set(gcf, 'Name', ['Results: ',imagefile], 'NumberTitle', 'Off')
set(gcf, 'Units', 'Normalized', 'OuterPosition', [0 0 1 1])
legend('Scratch Toughness (10^{-3} MPa*m^{1/2})','Scratch Hardness
(10^{-3} GPa)', 'Frictional Load (10^{-2} N)', 'Scratch Width (um)')
xlabel('Scratch Position (mm)')
```

```
datafinal=[pos,dataFin(:,2),dataFin(:,3),frac,hardness];
% Calculate Statistics about kIC & Hardness

avkIC=mean(frac);
stdkIC=std(frac);
avHardness=mean(hardness);
stdHardness=std(hardness);
dim = [.2 .6 .3 .3];
str = ['Scratch Toughness = ',num2str(avkIC),' ',char(177),'
',num2str(stdkIC),' MPa*m^{1/2}',char(10),...
    'Scratch Hardness = ',num2str(avHardness),' ',char(177),'
',num2str(stdHardness),' GPa'];
annotation('textbox',dim,'String',str,'FitBoxToText','on');

% Save results

exportDir='Results Plots\'; % If you are getting error code: undefined
export_fig, add the export_fig folder to the path!
saveas(handle3,[exportDir,name,'_ResultsPlot'],'fig')
export_fig(handle3,[exportDir,name,'_ResultsPlot'],'-jpg')
saveas(handle1,[exportDir,name,'_ImageAnalysis'],'fig')
export_fig(handle1,[exportDir,name,'_ImageAnalysis'],'-jpg')
fid=fopen([exportDir,name,'_Data.txt'],'wt');
fprintf(fid,'Position (m), Frictional Load (N), Scratch Width (m),
Scratch Toughness (MPa*m^1/2), Hardness (GPa)\n');
dlmwrite([exportDir,name,'_Data.txt'],datafinal,'Delimiter',',','-
append')
```

Scratch Data Analysis Script “datamanip.m”

```
function
[data,fighandle2]=datamanip_v4(lvdtfile,lvdtFloor,fin,lengthSet,startIg
nore,LVDTcalInitOffset,LVDTcalEndOffset)
%LVDT and Load Cell data manipulator
%Required Inputs:
%   lvdtfile: path to data set
%   lvdtFloor: Lower bound for identification of start point of scratch
%   displacement in LVDT data
%   fin: Approximate ending micrometer displacement point
%Optional Inputs:
%   lengthSet: use for runs with long data sets, multiplies length to
%   determine area of interest (default 2/3)
%   startIgnore: # of points to ignore from the start. Insert '[]' if
not
%   using
%   LVDTcalInitOffset: # of points before start of scratch to select
reference load
%   value for stage load calibration.
%   LVDTcalEndOffset: # of points after end of scratch to reference
load
%   value for stage load calibration.
% Example input:
%   [dataDAQ]=datamanip_v4(agiPath,2.5,13.3,2/3,'[]',75,75);

% Initialization:
fontSize= 15;

%Import LVDT data
[e,b]=xlsread(lvdtfile,'B:E');
% [~,b]=xlsread(lvdtfile,'B:B');
% [c,~]=xlsread(lvdtfile,'C:C')
% [d,~]=xlsread(lvdtfile,'E:E')

b(1:11,:)=[];
b=b(:,1);
d=e(7:end,4);
c=e(7:end,2);
format='dd:HH:MM:SS:FFF';
[~,~,~,~,mm,ss]=datevec(b,format); %read time data into numerical
format
t=mm.*60+ss;
lvdt=horzcat(t,c,d);

%see original data
pascol=lvdt(:,3);
lvdtl=lvdt(:,2);
fighandle2=figure;
subplot(2,2,1)
```

```
plot(lvdtl)
hold on
plot(pascol.*1000)
hold off
set(gcf, 'Units', 'Normalized', 'OuterPosition', [0 0 1 1]);
set(gcf, 'Name', 'Load/LVDT Processing Steps', 'NumberTitle', 'Off')
title('Original Data', 'FontSize', fontSize);

pascol=25388.51343.*pascol-6.169744732; % Convert Load Data from VDC to
force (N)
data=horzcat(lvdtl,pascol);

%find start and end points of scratch test
lvdtend=fin/22*(3.257427+5.27507)-5.27507;
factor2=2/3;
if exist('lengthSet')
    if ~isempty(lengthSet)
        factor2=lengthSet;
    end
end
l=round(factor2*length(data));

if isempty('startIgnore')
    startIgnore=1;
end

if ~exist('startIgnore')
    startIgnore=1;
end
if exist('lvdtFloor')
    [lst,~]=peakfinder(data(startIgnore:l,1),0.0001,lvdtFloor,1);
else
    [lst,~]=peakfinder(data(startIgnore:l,1),0.0001,3.2,1);
end
LVDTcalInit=50;
if exist('LVDTcalInitOffset')
    if ~isempty(LVDTcalInitOffset)
        LVDTcalInit=LVDTcalInitOffset
    end
end
LVDTcalEnd=100;
if exist('LVDTcalEndOffset')
    if ~isempty(LVDTcalEndOffset)
        LVDTcalEnd=LVDTcalEndOffset;
    end
end
initLoad=data(lst(end)-LVDTcalInit,2)
data=data(lst(end):end,:); %delete data before startpoint
subplot(2,2,2)
```

```
plot(data); title('Data Before Startpoint deleted');
[lst,~]=peakfinder(data(:,1),0.0001,lvdtend,-1);
endLoad=data(lst(1)+LVDTcalEnd,2)
data=data(1:lst(1),:); %delete data after endpoint
subplot(2,2,3)
plot(data(:,1).*10)
hold on
plot(data(:,2))
title('Scratch Specific Data', 'FontSize', fontSize);

%convert lvdt to micrometer displacement (determined from calibration
% of LVDT)
data(:,1)=22.*(data(:,1)+5.27507)./(3.257427+5.27507);
%subtract elastic contribution from stage springs
m=(endLoad-initLoad)/(data(end,1)-data(1,1));
data(:,2)=data(:,2)-(m*(data(:,1)-data(1,1))+initLoad);
% data(:,2)=data(:,2)-(16.87382-0.45278.*data(:,1));
subplot(2,2,4)
plot(data)
title('Data With Stage Load Subtracted', 'FontSize', fontSize);
end
```

Scratch Toughness Analysis Script “kIC.m”

```
function [ kIC,hardness,d ] = kIC( data,vLoad )
%kIC Calculates average fracture toughness from data

% Inputs
% data: 3 column matrix with scratch position (m), frictional force
(N),
% scratch width (m)
% vLoad: vertical load (kg)

% Dependencies
% units.m

% Initialization
dim=size(data);
l=dim(1);
u=units;

%Calculate scratch hardness and fracture toughness data
wT=0.0002;
dT=wT*(1-sin(pi/3));
[hardness,kIC,d]=deal(zeros(l,1));
if exist('vLoad')
    if ~isempty(vLoad)
        loadV=vLoad;
    end
end
for i=1:l
    width=data(i,3);
    load=data(i,2);
    if width>wT %deep scratch (shape function combined sphere and cone)
        d(i)=dT+1/tan(pi/3)*(width/2-wT/2); %calculated depth of
% scratch
        p=pi/3*wT+2*(width/2-wT/2)/sin(pi/3); %perimeter of scratch
        a=pi/3*wT^2/2-wT/2*wT*sin(pi/3)+(width+wT)/2*(d(i)-dT);
% contact area of scratch
    else %shallow scratch (shape function is sphere)
        d(i)=wT-sqrt(wT^2-(width/2)^2);
        p=2*wT*asin(width/2/wT);
        alp=asin(width/2/wT);
        a=alp*wT^2-wT*width/2*cos(alp);
    end

% hardness(i)=load*24.98*101.971621298/(width/u.um)^2;
hardness(i)=loadV*24.98/(width)^2/10^9; %hardness in GPa
kIC(i)=load/(2*p*a)^0.5/10^6; %scratch toughness in MPa*m^.5
end
end
```

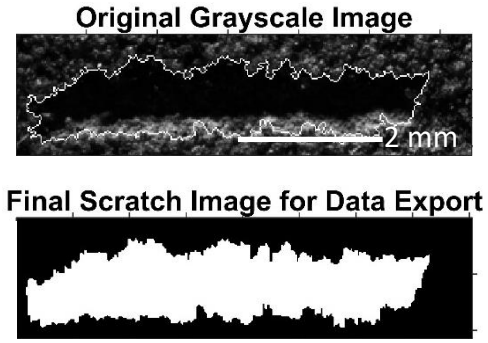

Figure B.1: Image analysis results for a scratched Entrada brine sample altered for two weeks in synthetic brine. The edge detection routines were completed using MatLab Image Processing Toolbox.

Appendix C: Schematics for Fabricated Scratch Test Apparatus Components

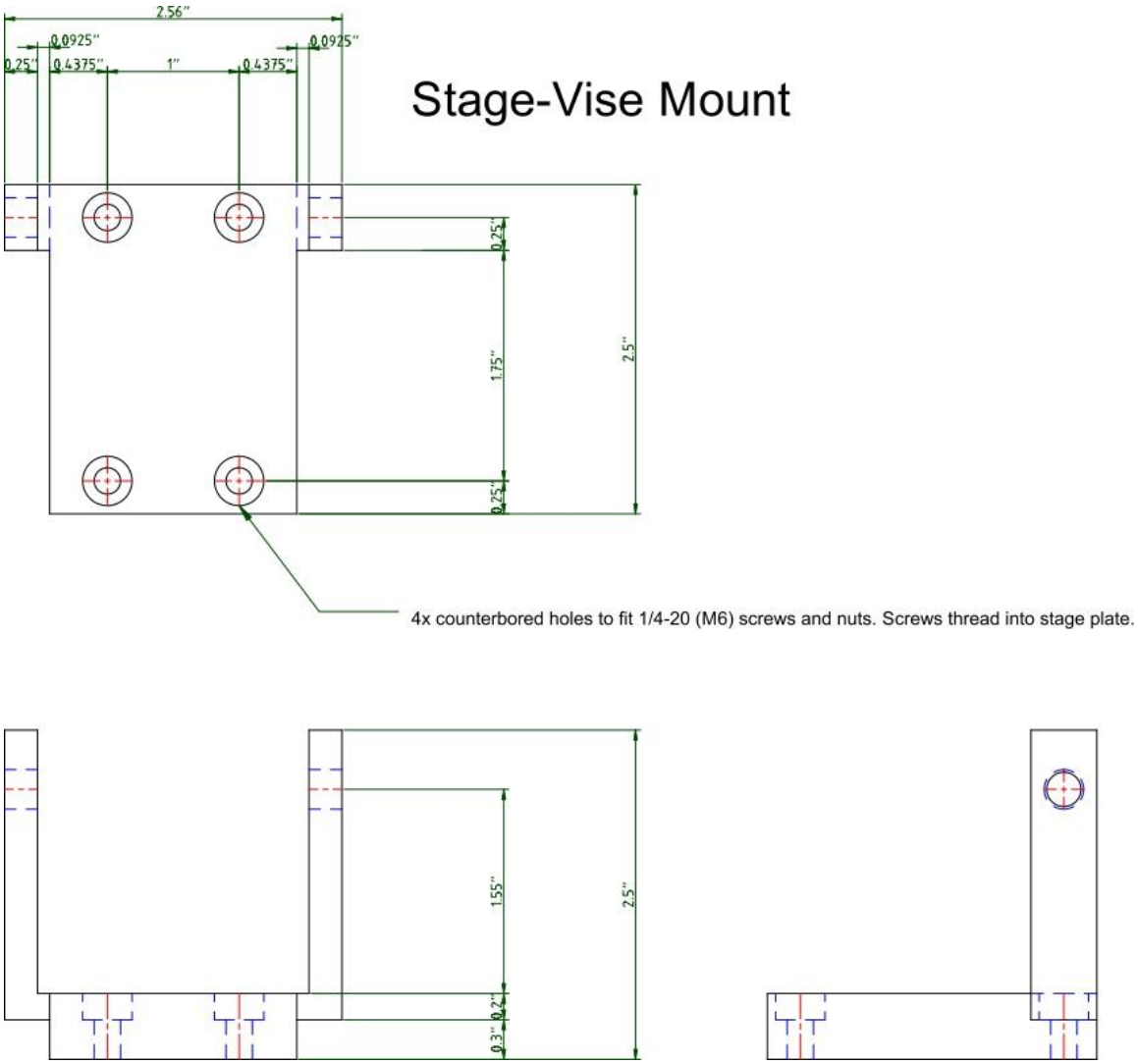

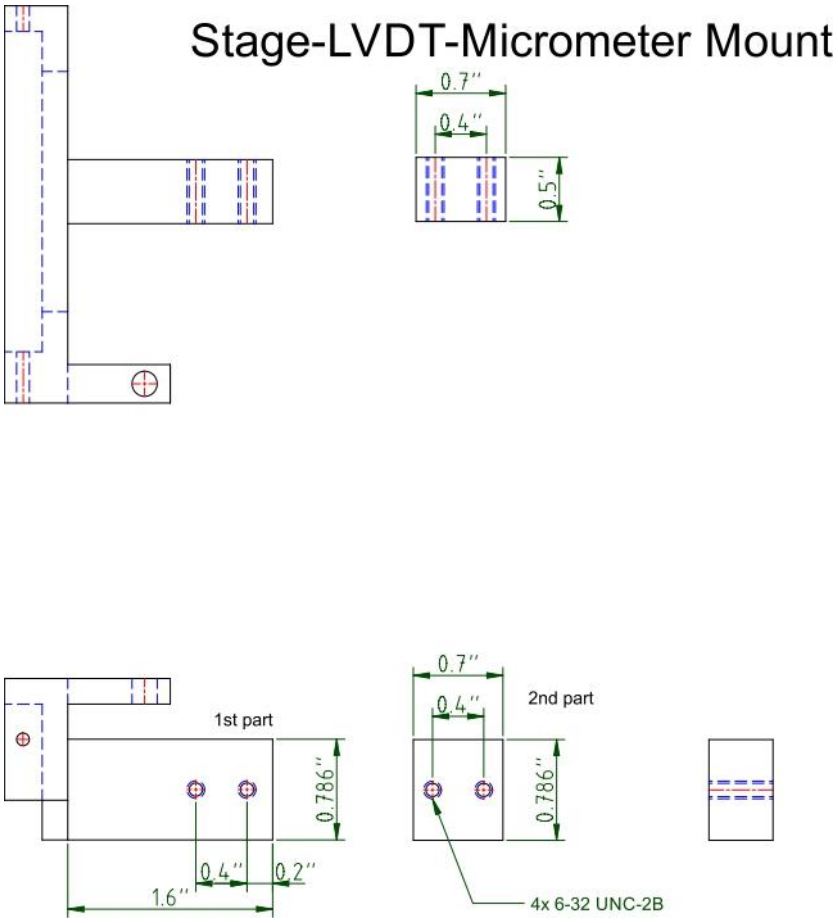
Stage-LVDT-Micrometer Mount
0.7''
0.4''
0.5''
1st part
0.786''
0.4''
0.2''
1.6''
0.7''
0.4''
2nd part
0.786''
4x 6-32 UNC-2B

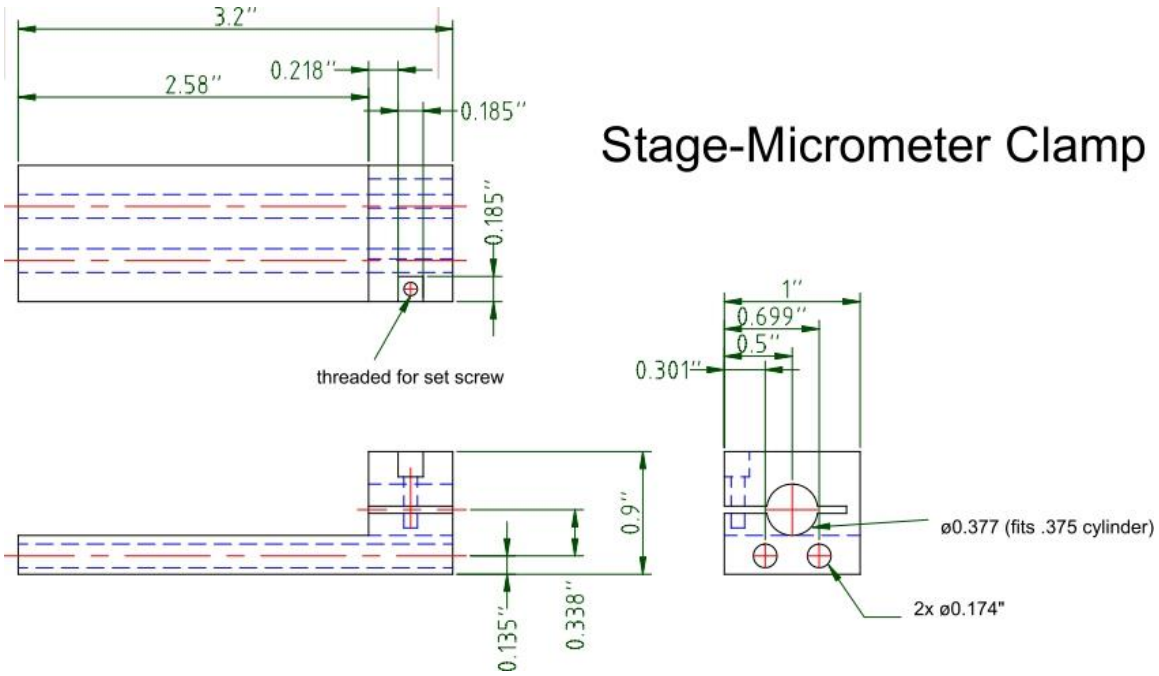

Illustration C.1: Fabricated Scratch Test Apparatus Components

References

Akono, a. T., Reis, P.M., Ulm, F.J., 2011. Scratching as a fracture process: From butter to steel. Phys. Rev. Lett. 106, 2–5. doi:10.1103/PhysRevLett.106.204302

Akono, A.-T., Ulm, F.-J., 2011. Scratch test model for the determination of fracture toughness. Eng. Fract. Mech. 78, 334–342. doi:10.1016/j.engfracmech.2010.09.017

Akono, A.T., Ulm, F.J., 2012. Fracture scaling relations for scratch tests of axisymmetric shape. J. Mech. Phys. Solids 60, 379–390. doi:10.1016/j.jmps.2011.12.009

Akono, A.-T., Randall, N.X., Ulm, F.-J., 2012. Experimental determination of the fracture toughness via microscratch tests: Application to polymers, ceramics, and metals. J. Mater. Res. 27, 485–493. doi:10.1557/jmr.2011.402

Altman, Y. (2017). Export_fig (https://www.mathworks.com/matlabcentral/fileexchange/23629), MATLAB Central File Exchange. Retrieved Feb, 2016.

Aslak, G. (2006). CutSamples (https://www.mathworks.com/matlabcentral/fileexchange/3447), MATLAB Central File Exchange. Retrieved Feb, 2016.

Bakker, E., Hangx, S.J., Niemeijer, A.R. and Spiers, C.J., 2016. Frictional behaviour and transport properties of simulated fault gouges derived from a natural CO 2 reservoir. International Journal of Greenhouse Gas Control, 54, pp.70-83.

Burnside, N.M., 2010. U-Th dating of travertines on the Colorado Plateau: implications for the leakage of geologically stored CO_2 [Ph.D. thesis]: Glasgow, Scotland, University of Glasgow, 290 p.

Canal, J., Delgado, J., Falcón, I., Yang, Q., Juncosa, R., Barrientos, V., 2013. Injection of CO_2-saturated water through a siliceous sandstone plug from the Hontomin test site (Spain): Experiment and modeling. Environ. Sci. Technol. 47, 159–167. doi:10.1021/es3012222

Carroll, S. a, McNab, W.W., Torres, S.C., 2011. Experimental Study of Cement - Sandstone/Shale - Brine - CO_2 Interactions. Geochem. Trans. 12, 9. doi:10.1186/1467-4866-12-9

Carroll, S., Hao, Y., Smith, M., Sholokhova, Y., 2013. Development of scaling parameters to describe CO_2-rock interactions within Weyburn-Midale carbonate flow units. Int. J. Greenh. Gas Control 16, S185–S193. doi:10.1016/j.ijggc.2012.12.026

Doelling, H.H., 2001, Geological Map of the Moab and Eastern part of the San Rafael Desert 30′ × 60′ quadrangles, Grand Emery Counties, Utah, and Mesa County Colorado: Utah Geological Survey Map 180.

Harding, D.S., Oliver, W.C. and Pharr, G.M. (1994) 'Cracking During Nanoindentation and its Use in the Measurement of Fracture Toughness', MRS Proceedings, 356. doi: 10.1557/PROC-356-663.

Kampman, N., Busch, A., Bertier, P., Snippe, J., Hangx, S., Pipich, V., Di, Z., Rother, G., Harrington, J.F., Evans, J.P., Maskell, A., Chapman, H.J., Bickle, M.J., 2016. Observational evidence confirms modelling of the long-term integrity of CO_2-reservoir caprocks. Nat. Commun. 7, 12268. doi:10.1038/ncomms12268

Kaszuba, J.P., Janecky, D.R., Snow, M.G., 2005. Experimental evaluation of mixed fluid reactions between supercritical carbon dioxide and NaCl brine: Relevance to the

integrity of a geologic carbon repository. Chem. Geol. 217, 277–293. doi:10.1016/j.chemgeo.2004.12.014

Kim, S., & Santamarina, J.C. (2014). CO_2 geological storage: Hydro-chemo-mechanical analyses and implications. *Greenhouse Gases: Science and Technology, 4*(4), 528-543.

Kitchin, J. (2012). Units for Matlab (https://www.mathworks.com/matlabcentral/fileexchange/36878), MATLAB Central File Exchange. Retrieved Feb, 2016.

Lau, D. (2000). Magicwand (https://www.mathworks.com/matlabcentral/fileexchange/130), MATLAB Central File Exchange. Retrieved Feb, 2016.

Le Guen, Y., Renard, F., Hellmann, R., Brosse, E., Collombet, M., Tisserand, D., Gratier, J.-P., 2007. Enhanced deformation of limestone and sandstone in the presence of high P co 2 fluids. J. Geophys. Res. 112, B05421. doi:10.1029/2006JB004637

Lu, J., Kharaka, Y.K., Thordsen, J.J., Horita, J., Karamalidis, A., Griffith, C., Hakala, J.A., Ambats, G., Cole, D.R., Phelps, T.J., Manning, M. a., Cook, P.J., Hovorka, S.D., 2012. CO_2–rock–brine interactions in Lower Tuscaloosa Formation at Cranfield CO_2 sequestration site, Mississippi, U.S.A. Chem. Geol. 291, 269–277. doi:10.1016/j.chemgeo.2011.10.020

Lüttge, A., & Metz, P. (1993). Mineralogy and Mechanism and kinetics of the reaction : a comparison of rock-sample and of powder experiments, 155–164.

Major, J. R., Eichhubl, P., Dewers, T. a., Urquhart, a. S., Olson, J. E., & Holder, J. (2014). The effect of CO 2 -related diagenesis on geomechanical failure parameters : fracture

testing of CO 2 -altered reservoir and seal rocks from a natural analog at Crystal Geyser , Utah. 48th US Rock Mechanics / Geomechanics Symposium.

Miller, M., Bobko, C., Vandamme, M., Ulm, F.J., 2008. Surface roughness criteria for cement paste nanoindentation. Cem. Concr. Res. 38, 467–476. doi:10.1016/j.cemconres.2007.11.014

Pokrovsky, O.S., Golubev, S. V., Schott, J., 2005. Dissolution kinetics of calcite, dolomite and magnesite at 25 °C and 0 to 50 atm p. CO_2 Chem. Geol. 217, 239–255. doi:10.1016/j.chemgeo.2004.12.012

Rinehart, A. (2015). Impact of microstructurally heterogeneous strength and compliance on macroscopic rock failure and elastic degradation. *PhD Dissertation. New Mexico Institute of Mining and Technology*.

Rohmer, J., Pluymakers, A., Renard, F., 2016. Mechano-chemical interactions in sedimentary rocks in the context of CO_2 storage: Weak acid, weak effects? Earth-Science Rev. 157, 86–110. doi:10.1016/j.earscirev.2016.03.009

Salter, C. (2000). Error Analysis Using the Variance-Covariance Matrix. Journal of Chemical Education, 77(9), 1239. http://doi.org/10.1021/ed077p1239

Schei, G., Fjaer, E., Detournay, E., Kenter, C.J., Fuh, G.F., Zausa, F., 2000. The Scratch Test: An Attractive Technique for Determining Strength and Elastic Properties of Sedimentary Rocks. SPE Annu. Tech. Conf. Exhib. 1–7. doi:10.2118/63255-MS

Shin, H., Santamarina, J. C., & Cartwright, J. A. (2008). Contraction-driven shear failure in compacting uncemented sediments. Geology, 36(12), 931-934.

Stumm, W., & Morgan, J. (1996). *Aquatic chemistry: Chemical equilibria and rates in natural waters* (3rd ed.). New York: Wiley, page 150-157.

Sun, Y., Aman, M., & Espinoza, D. N. (2016). Assessment of mechanical rock alteration caused by CO_2–water mixtures using indentation and scratch experiments. International Journal of Greenhouse Gas Control, 45, 9–17. http://doi.org/10.1016/j.ijggc.2015.11.021

Wanty, R. B., Pitman, J. K., & Fouch, T. D. (1991). Ground-water chemistry and diagenetic reactions in Tertiary sandstones of the Green River and Wasatch formations, Uinta Basin, Utah. U. S. Geological Survey Bulletin, X1–X21.

Wigley, M., Kampman, N., Dubacq, B., Bickle, M., 2012. Fluid-mineral reactions and trace metal mobilization in an exhumed natural CO_2 reservoir, Green River, Utah. Geology 40, 555–558. doi:10.1130/G32946.1

Yoder, N. (2016). Peakfinder (https://www.mathworks.com/matlabcentral/fileexchange/25500) MATLAB Central File Exchange. Retrieved Feb, 2016.